



Review

Radiation-Driven Wind Hydrodynamics of Massive Stars: A Review

Michel Curé ^{1,*}  and Ignacio Araya ² ¹ Instituto de Física y Astronomía, Universidad de Valparaíso, Gran Bretaña 1111, Valparaíso 2340000, Chile² Vicerrectoría de Investigación, Universidad Mayor, Santiago 8580745, Chile; ignacio.araya@umayor.cl

* Correspondence: michel.cure@uv.cl

Abstract: Mass loss from massive stars plays a determining role in their evolution through the upper Hertzsprung–Russell diagram. The hydrodynamic theory that describes their steady-state winds is the line-driven wind theory (m-CAK). From this theory, the mass loss rate and the velocity profile of the wind can be derived, and estimating these properly will have a profound impact on quantitative spectroscopy analyses from the spectra of these objects. Currently, the so-called β law, which is an approximation for the fast solution, is widely used instead of m-CAK hydrodynamics, and when the derived value is $\beta \gtrsim 1.2$, there is no hydrodynamic justification for these values. This review focuses on (1) a detailed topological analysis of the equation of motion (EoM), (2) solving the EoM numerically for all three different (fast and two slow) wind solutions, (3) deriving analytical approximations for the velocity profile via the LambertW function and (4) presenting a discussion of the applicability of the slow solutions.

Keywords: stars: massive; stars: mass-loss; hydrodynamics; analytical methods; numerical methods

**Citation:** Curé, M.; Araya, I.

Radiation-Driven Wind

Hydrodynamics of Massive Stars: A

Review. *Galaxies* **2023**, *11*, 68.[https://doi.org/10.3390/](https://doi.org/10.3390/galaxies11030068)[galaxies11030068](https://doi.org/10.3390/galaxies11030068)

Academic Editor: Artemio Herrero

Received: 14 March 2023

Revised: 5 May 2023

Accepted: 9 May 2023

Published: 12 May 2023

**Copyright:** © 2023 by the authors.

Licensee MDPI, Basel, Switzerland.

This article is an open access article

distributed under the terms and

conditions of the Creative Commons

Attribution (CC BY) license ([https://](https://creativecommons.org/licenses/by/4.0/)[creativecommons.org/licenses/by/](https://creativecommons.org/licenses/by/4.0/)

4.0/).

1. Introduction

At the beginning of the XX Century, Johnson [1,2] and Milne [3] argued that the force exerted on ions in the atmosphere of a luminous star could be responsible for the ejection of these ions from the star. They also argued that the ejected ions should carry with them the corresponding number of electrons, and strictly there should be no charge current, but they did not realize at that time that the collisional coupling between ions and protons would drag the rest of the plasma (mostly fully ionized hydrogen) with them as well, at least to supersonic velocities, and this theory was laid aside. It was Chandrasekhar [4,5] who, in the context of globular cluster dynamics, developed the theory of collisions due to an inverse square law, and Spitzer [6] applied Chandrasekhar's theory for collisions between charged particles.

Morton [7] was the first to report far-ultraviolet observations of three OB supergiants from an Aerobee-sounding rocket. After this came *Copernicus*, the first satellite with a telescope on board, and since then it has been possible to obtain stellar spectra in the ultraviolet (UV) region. Morton [7] found that the resonance lines of C IV, N V and Si IV showed the typical P-Cygni profiles (see Lamers and Cassinelli [8], Section 2.2). He found that the displacements in the profiles of C IV $\lambda\lambda 1549.5$ and Si IV $\lambda\lambda 1402.8$ corresponded to outflow velocities in the range of 1500–3000 km/s.

Snow and Morton [9] showed through a detailed survey that stars brighter than $M_{bol} \sim -6$ have strong P-Cygni profiles in their spectra and therefore *lose mass*. The same conclusion was arrived at by Abbott [10], who compared the radiative force with the gravitational force and concluded that radiative forces could initialize and maintain the mass loss process for stars with an initial mass at the zero-age main sequence (ZAMS) of about $15 M_{\odot}$ or greater.

This mass loss process (known as stellar wind), together with supernovae explosions, are the main contributors in supplying the interstellar medium (ISM) with nuclear-processed

heavy elements and therefore influence not only chemical evolution (and therefore star formation) but also the energy equilibrium of the ISM and the Galaxy (see [11–13] and the references therein).

Parker [14] was the first to develop the notion of solar wind through a purely gas dynamical theory, which was the only known stellar wind theory until the winds of massive stars were discovered. When this theory was applied to the winds of a typical O-star, the effective temperature necessary to reproduce the observed terminal velocities was of the order of 10^7 K, a value that is completely excluded by the presence of lines such as Si IV, C IV and N V ions, which would be destroyed by collisional ionization at temperatures above 3×10^5 K. It was, therefore, necessary to seek an alternative mechanism to drive the wind. The natural driven mechanism is the force due to the interaction of the radiation field on the wind plasma, and the simplest form is the force due to the continuum, i.e., the Thompson radiative acceleration. This force leads macroscopically to a decrease in the star's gravitational attraction by a constant factor (for O-stars this is between 0.3 and 0.6). It is then clear that the continuum force alone cannot produce a force that exceeds gravity and, therefore, cannot drive these kinds of winds.

Lucy and Solomon [15] resuscitated the proposal of Johnson and Milne and considered the force due to the absorption of spectral lines, but unlike the earlier authors, they considered the flow of the plasma as a whole rather than as the selective ejection of specific ions. They calculated an upper limit on the force on the C IV line $\lambda\lambda 1548$, finding that this exceeds the force of gravity by a factor of approximately a few hundred. Hydrostatic equilibrium in the outermost layers is not possible, and an outflow of material must occur. In their stellar wind model, Lucy and Solomon made a series of assumptions, for instance, that the wind is driven only by resonance lines. They found mass loss rates for O-stars of two orders of magnitudes less than the values obtained from observations.

A significant step in the theory was made by Castor, Abbot and Klein [16] (hereafter CAK), who realized that the force due to line absorption in a rapidly expanding envelope could be calculated using the Sobolev approximation [17,18]. Then, by developing a simple parameterization of the line force using the point star approximation, they were able to construct an analytical wind model. Despite the number of approximations made in that work, e.g., they represented the line force by C III lines and calculated only one model for a typical O5 f star ($T_{\text{eff}} = 49,290$ K, $\log g = 3.94^1$ and $R/R_{\odot} = 13.8$), they obtained a mass loss rate of $\dot{M} = 6.61 \times 10^{-6} M_{\odot}/\text{year}$ and a terminal velocity of $v_{\infty} = 1515$ km/s. The value of the mass loss rate was of the same order of magnitude as the values obtained from observations, but the terminal velocity lay below the measured ones. They also gave analytical scaling relations for the mass loss rates and terminal speeds as functions of the stellar parameters. These were widely used to prove (or disprove) the validity of the radiation-driven (or line-driven) wind theory by comparison with the observations.

Abbott [10] improved this theory by calculating the line force using a tabulation of ca. 250,000 lines, which was complete for the elements H to Zn in the ionization states I to VI. Currently, the non-local thermodynamic equilibrium code CMFGEN [20] uses around 900,000 lines and FASTWIND contains 4 million lines [21] (see also [22], which uses ca. 4 million lines). Despite this immense effort to give a more realistic representation of the line force, evident discrepancies with the observations remained. Simultaneously and independently, Friend and Abbott [23] and Pauldrach et al. [24] calculated the influence of the finite cone angle correction on the dynamics of the wind (described in the Appendix from [18]). They found a much better agreement between the improved or modified CAK theory (hereafter m-CAK) and the observations of the mass loss rate and the terminal velocity in a large domain in the Hertzsprung–Russell diagram.

The equation of motion of the m-CAK theory is a highly non-linear differential equation that has singular points, eigenvalues and solution branches (see [16,23–27]). Since it is challenging to solve this differential equation numerically, Pauldrach et al. [24] found that the velocity field, $v(r)$, from the m-CAK theory can be described by a simple approximation, known as the β law approximation (see below). In

addition, Kudritzki et al. [28] developed analytical approximations for the localization of the critical point, mass loss rate and terminal velocity with an agreement within 5% for v_∞ and 10% for \dot{M} when compared to the correct numerical calculations.

Radiation-driven stellar winds are hydrodynamic phenomena involving the flow of the outer layers of the atmospheres of massive stars. This review is focused on describing the investigation of the m-CAK hydrodynamic theory, its topology and its three known physical solutions.

Section 2 presents the theory to calculate the radiation (line) force via an analytical description thanks to the Sobolev approximation. Section 3 introduces the m-CAK hydrodynamic theory, and its topological description is given in Section 4. Section 5 shows all three known physical solutions, whilst Section 6 presents analytical approximate solutions based on the LambertW function. Finally, in Section 7, we summarise the main topics of this review and discuss the applicability of slow solutions.

2. The Radiation Force

The exact calculation of the radiation force requires a knowledge of the radiation field (in all the lines and continua) and of the physical processes (scattering, absorption and emission) that contribute to the exchange of energy and momentum throughout the wind. The radiation field is represented by the monochromatic specific intensity $I_\nu(\mu)$, where μ is the cosine of the angle between the incoming beam and the velocity vector of the interacting particles. Thus, the radiation force per unit of volume at a distance r exerted on a point particle per unit of time is equal to the momentum removed from the incident radiation field ($\kappa\rho I(\mu) \mu/c$) integrated over all the scattering directions. This force is given by

$$\mathbf{F}^{\text{rad}}(r) = \frac{4\pi}{c} \frac{1}{2} \int_0^\infty \int_{-1}^1 \kappa_\nu(r) \rho(r) I_\nu \mu d\mu d\nu, \quad (1)$$

where the absorption coefficient κ_ν is given in units of $\text{cm}^2 \text{g}^{-1}$. The net flux density comes from the interaction processes integrated over the whole spectral range between the radiation field emitted by the photosphere and the stellar wind of mass density ρ at the distance r . Here, it is assumed that the emissivity (thermal emission and photon scattering) in the expanding atmosphere is isotropic. Therefore, no net momentum change occurs from this process (see [29], Chapter 20).

The absorption coefficient κ_ν consists of three main contributions:

$$\kappa_\nu = \kappa^{\text{Th}} + \kappa_\nu^{\text{cont}} + \kappa_\nu^{\text{line}}, \quad (2)$$

where κ^{Th} represents the Thomson scattering, κ_ν^{cont} is the contribution of bound-free and free-free transitions and κ_ν^{line} is the sum of all line absorption coefficients at frequency ν .

The radiation force can be calculated by state-of-the-art non-local thermodynamic equilibrium (NLTE) radiative transfer codes such as FASTWIND [30,31], CMFGEN [20,32–34] or POWR [35,36], but these calculations depend on the velocity and density profile used to describe the wind.

2.1. Radiative Force Due to Electron Scattering

The interaction between photons and free electrons is described by a Compton process (an excellent review of this process, including Monte Carlo calculations, can be found in [37]). If photons with energy $h\nu \ll m_e c^2$ are scattered by Maxwellian electrons² with $kT \ll m_e c^2$, the frequency shift will be very small, but if the scattering process is repeated many times, the small amounts of energy exchanged between the electrons and photons can build up and give rise to substantial effects.

In the non-relativistic limit without the influence of quantum effects ($h\nu \ll m_e c^2$) and neglecting the possible effects described above, the scattering cross-section is frequency independent and called the Thomson cross-section, namely:

$$\sigma^{\text{Th}} = \frac{8\pi}{3} \frac{e^4}{m_e^2 c^4}. \quad (3)$$

The value of this cross-section is $\sigma^{\text{Th}} = 6.65 \times 10^{-25} \text{ cm}^2$ and the absorption coefficient is therefore:

$$\kappa^{\text{Th}} \rho = n_e \sigma^{\text{Th}}. \quad (4)$$

Using this value (κ^{Th}) in Equation (2) and integrating Equation (1), we obtain the contribution of Thomson scattering to the radiation force,

$$\mathbf{F}^{\text{Th}} = n_e \frac{\sigma^{\text{Th}} L}{4\pi c r^2}, \quad (5)$$

where L is the luminosity of the star. The radiative acceleration on the electrons is then

$$g_e^{\text{Th}} = \frac{1}{m_e} \frac{\sigma^{\text{Th}} L}{4\pi c r^2}. \quad (6)$$

It is useful to define the ratio of the Thomson scattering force and the gravitational force by:

$$\Gamma_e = \frac{g_e^{\text{Th}}}{g^{\text{grav}}} = \frac{1}{m_e} \frac{\sigma^{\text{Th}} L}{4\pi c G M_*}, \quad (7)$$

where G is the gravitational constant and M_* is the star's mass. In the standard one-component description of stellar winds, the force over the density of the plasma is given by:

$$g^{\text{Th}} = \left(\frac{n_e}{\rho} \right) \frac{\sigma^{\text{Th}} L}{4\pi c r^2} \quad (8)$$

where $\rho = m_p n_p + \sum_{\text{ions}} (m_i n_i) + n_e m_e$ is the mass density. The principal contribution of the ions comes from helium, and neglecting the electrons, $n_e m_e$, the density is

$$\rho \simeq m_p n_p (1 + A_{\text{He}} Y_{\text{He}}). \quad (9)$$

Here, A_{He} is the atomic mass of a helium atom, Y_{He} is the relative abundance of helium with respect to hydrogen (the latter being described by the subscript p) and m_p is the proton mass. Based on the conservation of charge, it is possible to express the electron number density as $n_e = n_p (1 + q_{\text{He}} Y_{\text{He}})$, where $q_{\text{He}} = 0, 1$ or 2 depending on the helium ionisation state.

Thus, the ratio n_e/ρ is:

$$\frac{n_e}{\rho} = \frac{1}{m_p} \left(\frac{1 + q_{\text{He}} Y_{\text{He}}}{1 + A_{\text{He}} Y_{\text{He}}} \right) \quad (10)$$

and the acceleration is:

$$g^{\text{Th}} = \frac{1}{m_p} \left(\frac{1 + q_{\text{He}} Y_{\text{He}}}{1 + A_{\text{He}} Y_{\text{He}}} \right) \left(\frac{\sigma^{\text{Th}} L}{4\pi c r^2} \right) \quad (11)$$

or

$$\Gamma_e = \left(\frac{1 + q_{\text{He}} Y_{\text{He}}}{1 + A_{\text{He}} Y_{\text{He}}} \right) \left(\frac{\sigma^{\text{Th}} L}{4\pi c m_p G M_*} \right). \quad (12)$$

Quite often, the canonical value of $\kappa^{\text{Th}} = 0.34 \text{ cm}^2 \text{ g}^{-1}$ is adopted, which follows from assuming a fully ionised plasma at solar abundance. In addition, since the continuum of OB

stars is also optically thin in the lines near its maximum, the contribution of the continuum to the total radiative force is neglected.

The next section provides a general description of the line force based on the Sobolev approximation (see, e.g., Lamers and Cassinelli [8] or Hubeny and Mihalas [29]).

2.2. Radiative Force due to Lines

The contribution to the radiation force due to the spectral lines in the wind of massive stars is provided by the momentum transfer of photons (via absorption and re-emission processes in optically thick lines) mainly from the most dominant ions (i.e., C, O, N and the Fe group). The proper calculation of the line force (per unit volume) is given by:

$$F^{\text{line}}(r) = \frac{2\pi}{c} \sum_l \int_0^\infty \int_{-1}^{+1} \kappa_l(r) \rho(r) \phi_l(v, \mu, r) I_\nu(r, \mu) \mu d\mu dv \quad (13)$$

where ϕ is the Gaussian absorption profile. The summation is over all the line transitions (l), assuming non-overlapping lines, for which the wind is optically thick. κ_l is the opacity coefficient (in $\text{cm}^2 \text{g}^{-1}$) of lines formed between levels l (lower) and u (upper) with energy $h\nu_0$,

$$\kappa_l \rho = \frac{\pi e^2}{m_e c} f_l n_l \left(1 - \frac{n_u g_l}{n_l g_u} \right). \quad (14)$$

The number densities n_l and n_u of ions in levels l and u are given in cm^{-3} , g_l and g_u are the corresponding statistical weights and f_l is the oscillator strength of the line. The CAK theory allows us to find an analytical expression for the line force in a moving media with large velocity gradients in terms of the macroscopic variables using the Sobolev approximation. However, this expression only applies to radiating flows in the non-relativistic regime.

2.2.1. The Sobolev Approximation

In a moving plasma such as stellar wind, the interaction of radiation with matter can be better understood as follows. Let us consider a single spectral line thermally broadened with a rest wavelength λ_1 . A photon emitted from the stellar surface with wavelength $\lambda_* < \lambda_1$ propagates without interacting with the matter until, due to the Doppler shift, it is scattered at the blue edge of the line in question. Due to the expansion of the wind, the particles viewed from any direction from a certain position always appear to be receding. This means that independent of the scattered direction of the photon (forward or backwards), the distance travelled always causes its comoving wavelength to be red shifted.

After many scatterings, the photon's wavelength has been shifted to the line's red edge, and the interaction of this photon with the line (λ_1) ceases. The region in the wind where an incoming photon can interact with the ions is called the interaction zone. It is also well known that the winds of massive stars reach terminal velocities of several times the sound speed, and the point at which the wind velocity is equal to the sound speed (the sonic point) is very near to the photosphere. This means that almost all the region where stellar winds are found is supersonic.

This description corresponds to the Sobolev approximation [17], where all the relevant physical quantities, such as the opacity, source function, etc., are considered constant in the interaction zone, i.e., the width of the interaction zone is small compared with a characteristic flow length. Thus, for a generic Doppler-broadened line profile, the Sobolev length, L_s , is defined as:

$$L_s = v_{\text{th}} / (dvs./dr), \quad (15)$$

where T_{eff} is the star's effective temperature, $v_{\text{th}} = \sqrt{2k_B T_{\text{eff}}/m_p}$ is the thermal speed of the protons and k_B is the Boltzmann constant.

A characteristic length of the flow is

$$L_c \simeq v s. / (dv s. / dr) \quad (16)$$

Typical values of thermal velocities in OB-type stars are about 7–20 km/s, while terminal velocities are about 1000–3000 km/s (see, e.g., Lamers and Cassinelli [8], Puls et al. [12]). More recent measurements of terminal velocities based on observations performed in the frame of the ULLYSES collaboration [38] have been accomplished by Hawcroft et al. [39].

2.2.2. The Line Force due to a Single Line

Castor [18] analysed the Sobolev approximation in detail in the context of stellar winds and showed that the force produced by the incoming radiation due to a single line can be expressed as³:

$$f^{\text{line}} = \left(\frac{F_\nu \Delta \nu_d}{c} \right) \left(\frac{k_l}{\tau_l} \right) (1 - e^{-\tau_l}), \quad (17)$$

where $\Delta \nu_d = v_{\text{th}} \nu / c$ corresponds to the Doppler shift, F_ν is the flux of the radiation field at frequency ν , k_l is the monochromatic line absorption coefficient per unit mass and

$$\tau_l = \int \rho \phi(\nu, r) k_l dr \quad (18)$$

is the optical depth. Evaluating the optical depth for a normalized Gaussian profile and using the Sobolev approximation, we find:

$$\tau_l = k_l \rho v_{\text{th}} / (dv s. / dr). \quad (19)$$

With this expression, we can interpret the RHS of (17) as:

- (i) $(F_\nu \Delta \nu_d / c)$ is the rate of momentum emitted by the star per unit area at frequency ν with bandwidth $\Delta \nu_d$;
- (ii) $(\tau_l / k_l) = \rho v_{\text{th}} / (dv / dr)$ represents the amount of mass that can absorb this momentum;
- (iii) $(1 - e^{-\tau_l})$ is the probability that such an absorption occurs.

Then, we define

$$t = \sigma_e \rho v_{\text{th}} / (dv / dr), \quad (20)$$

where $\sigma_e = \sigma^{\text{Th}} n_e / \rho$ corresponds to the Thomson scattering absorption coefficient per density. In a moving medium, t represents the optical depth that a line will have if its opacity is equal to its electron scattering opacity. Based on this definition, it is possible to rewrite t as

$$\tau_l = \eta_l t \quad (21)$$

where $\eta_l = k_l / \sigma_e$. The first factor in (21) is related only to line properties, and the second only to dynamic variables of the wind.

2.2.3. The Line Force due to a Statistical Distribution of Line Strength

The total line force due to the addition of all the single lines of the ions for a point star approximation and for non-overlapping single lines is given by:

$$f^{\text{line}} = \sum_l \left(\frac{F_\nu \Delta \nu_d}{c} \right)_l \left(\frac{dv / dr}{\rho v_{\text{th}}} \right) (1 - e^{-\eta_l t}). \quad (22)$$

Expressing (22) in terms of $\Delta \nu_d = \nu v_{\text{th}} / c$ and the relation $F = L / 4\pi r^2$, we obtain

$$f^{\text{line}} = \frac{L}{c^2} \left(\frac{dv / dr}{4\pi r^2} \right) \sum_l \left(\frac{L_\nu \nu}{L} \right)_l (1 - e^{-\eta_l t}) \quad (23)$$

Abbott [10] was the first to compile and publish a list of ca. 250,000 lines for atoms from H to Zn in ionisation stages I to VI. Based on such a line list [22,40,41], it is possible to derive a line strength distribution function [24,42]. This distribution can be described as follows:

$$dN(k_l) = \int_0^N \left(\frac{L_v v}{L} \right) n(k_l, v) dv \quad (24)$$

and represents the number of lines in the line strength interval $(k_l, k_l + \Delta k_l)$ obtained from the total spectrum and weighted by the flux mean of line strength $(L_v v / L)$. Notice that in Equation (24), the distribution in frequency space of the lines is independent from the distribution in line strength. An alternative formulation of the line statistic is given by Gayley [43] (see also [22]).

The logarithm of the number of lines can be fitted by a linear function, namely:

$$dN(k_l) = N_0 (1 - \alpha) (k_l / \sigma_e)^{\alpha-2} d(k_l / \sigma_e) \quad (25)$$

where N_0 is the number of lines (strong and weak) that effectively contribute to the line force. Typical values of the parameter α are $0.45 \leq \alpha \leq 0.7$ [8,42]. Notice that line force parameters are not free but depend on the transfer problem in each individual star (see [22,41,42,44–46], for a detailed description of the calculation of the line force parameters).

Extending the sum in Equation (23) to an integral, we obtain the line force expression:

$$f^{\text{line}} = \frac{L}{c^2} \frac{(dv/dr)}{4\pi r^2} N_0 (1 - \alpha) \int_{\sigma_e}^{\infty} (1 - e^{-\eta t}) (k_l / \sigma_e)^{(\alpha-2)} d(k_l / \sigma_e). \quad (26)$$

Neglecting the lower limit of the integral, a valid approximation for stars of type OB, and replacing it by zero and integrating, the line force becomes:

$$f^{\text{line}} = \frac{L}{c^2} \frac{1}{4\pi r^2} v_{\text{th}} \sigma_e N_0 (1 - \alpha) \Gamma(\alpha) \left(\frac{dv/dr}{\sigma_e \rho v_{\text{th}}} \right)^{\alpha}, \quad (27)$$

where Γ is the Γ -function. Then, dividing by the total density, we obtain the standard form of the line acceleration,

$$g^{\text{line}} = \frac{C}{r^2} \left(r^2 v \frac{dv}{dr} \right)^{\alpha}, \quad (28)$$

with

$$C = \Gamma_e G M_* k \left(\frac{4\pi}{\sigma_e v_{\text{th}} \dot{M}} \right)^{\alpha}, \quad (29)$$

where Γ_e is the radiative acceleration due to Thomson scattering in terms of the gravitational acceleration and \dot{M} is the mass loss rate. Here, the continuity equation has been used, and the variables, such as N_0 or $\Gamma(\alpha)$, have been collected into the constant k . Note that this expression for the line force (Equation (28)) only takes interactions between ions and radially emitted photons into account [16,18].

2.2.4. The Correction Factor

Castor et al. [16] (see their appendix) qualitatively discussed the effect on the line force that the proper shape of the star (non-radial incoming photons) would have on the wind kinematics. Later Pauldrach et al. [24] and Friend and Abbott [23] independently investigated the influence of this effect, known as the finite disc correction factor, thereby developing the m-CAK theory.

The expression of the line force for incoming photons from an arbitrary direction for a radial flow velocity field comes from the definition of Equation (20); thus,

$$t_{\sigma} = \left(\frac{1 + \sigma}{1 + \mu^2 \sigma} \right) \frac{\sigma_e \rho v_{\text{th}}}{dv/dr}, \quad (30)$$

where

$$\sigma = \frac{d \ln v s.}{d \ln r}. \quad (31)$$

Inserting t_σ into Equation (26) instead of t and integrating, we obtain the following expression for the line force:

$$g^{\text{line}} = \frac{C}{r^2} CF(r, v, v') (r^2 v v')^\alpha \quad (32)$$

where CF is the correction factor, defined as the ratio of the force due to the non-radial contributions to that of a point star approximation, namely:

$$CF = \frac{2}{1 - \mu_c^2} \int_{\mu_c}^1 \left[\frac{(1 - \mu^2) v/r + \mu^2 v'}{v'} \right]^\alpha \mu d\mu \quad (33)$$

with $\mu_c = \sqrt{(1 - R_*^2/r^2)}$, where R_* is the stellar radius and $v' = dv/dr$. In Appendix A, we summarised some properties of the correction factor.

2.3. The Ionization Balance

In their work, Abbott [10] assumed a local thermodynamic equilibrium (LTE) and used the modified Saha formula (see Hubeny and Mihalas [29]) to take the dilution of the radiation field and the possible difference between the electron kinetic temperature T_e and the radiation temperature T_r into account. Due to the changes in the ionisation throughout the wind, Abbott fitted the line force not only in terms of $(r^2 v s. v')^\alpha$ (see Equation (28)) but also as a function of the ratio $n_e/W(r)$, where

$$W(r) = \frac{1}{2} \left(1 - \sqrt{(1 - R_*^2/r^2)} \right) \quad (34)$$

is the dilution factor. They found that the functional dependence of this quotient in the line force is:

$$g^{\text{line}} \propto \left(\frac{n_e}{W(r)} \right)^\delta, \quad (35)$$

where the electron number density, n_e , is given in units of 10^{11} cm^{-3} . This proportionality means that the greater the density, the lower the ionisation level. In view of the fact that the lower ionisation levels have more line transitions, usually at the maximum of the radiation field, the line force increases with increasing density. Values of this δ line force parameter for the fast solution (see below) are in the range $0 < \delta \lesssim 0.2$ [8], but for a pure hydrogen atmosphere, the value is $\delta = 1/3$, as Puls et al. [42] demonstrated.

3. The m-CAK Hydrodynamic Model

The 1D m-CAK stationary model for line-driven stellar winds considers the following assumptions: an isothermal fluid in spherical symmetry and no influence from viscosity effects, heat conduction and magnetic fields.

The stationary continuity and momentum conservation equations are:

$$\dot{M} = 4 \pi r^2 \rho v s., \quad (36)$$

$$v \frac{dv}{dr} = -\frac{1}{\rho} \frac{dP}{dr} - \frac{GM_*(1 - \Gamma_e)}{r^2} + \frac{v_\phi^2(r)}{r} + g^{\text{line}}(\rho, dv/dr, n_e), \quad (37)$$

where P is the fluid pressure and $v_\phi = v_{\text{rot}} R_*/r$, with v_{rot} being the stellar rotational speed at the equator. In addition, $g^{\text{line}}(\rho, dv/dr, n_e)$ corresponds to the acceleration due to an ensemble of lines.

The standard or m-CAK parameterization of the line force [10,23,24] is the following:

$$g^{\text{line}} = \frac{C}{r^2} CF(r, v, dv/dr) \left(r^2 v \frac{dv}{dr} \right)^\alpha \left(\frac{n_e}{W(r)} \right)^\delta, \quad (38)$$

where the coefficient C is given in Equation (29).

Substituting the density from the mass conservation equation (Equation (36)) into the momentum equation (Equation (37)), we obtain the equation of motion (EoM).

Transforming to dimensionless variables, that is

$$u = -\frac{R_*}{r}, \quad (39)$$

$$w = \frac{v}{a}, \quad (40)$$

$$w' = \frac{dw}{du}, \quad (41)$$

where a is the isothermal sound speed of an ideal gas, $P = a^2 \rho$.

Using these new variables, the EoM now reads:

$$F(u, w, w') = \left(1 - \frac{1}{w^2} \right) w \frac{dw}{du} + A + \frac{2}{u} + a_{\text{rot}}^2 u - C' CF g(u) (w)^{-\delta} \left(w \frac{dw}{du} \right)^\alpha = 0, \quad (42)$$

where the constants are the following:

$$A = \frac{GM(1 - \Gamma_e)}{a^2 R_*} = \frac{v_{\text{esc}}^2}{2a^2}, \quad (43)$$

$$a_{\text{rot}} = \frac{v_{\text{rot}}}{a}, \quad (44)$$

$$C' = C \left(\frac{\dot{M} D}{2\pi a R_*^2} 10^{-11} \right)^\delta (a^2 R_*)^{(\alpha-1)}, \quad (45)$$

$$D = \frac{(1 + Z_{\text{He}} Y_{\text{He}})}{(1 + A_{\text{He}} Y_{\text{He}})} \frac{1}{m_p}, \quad (46)$$

where Z_{He} is the number of free electrons provided by helium, v_{esc} is the escape velocity and the function g is defined as:

$$g(u) = \left(\frac{u^2}{1 - \sqrt{1 - u^2}} \right)^\delta \quad (47)$$

In order to find a physical wind solution of the EoM (Equation (42)), i.e., starting from the photosphere with a small velocity and reaching infinity with a supersonic velocity, we first need to understand the topology of this equation.

4. Topological Analysis

As mentioned previously, the first wind model was developed by Parker [14] for the sun. This model possesses a singular point at the sonic point and different solution branches (see Figure 3.1 in [8]). The m-CAK model has a driving force (line force) that depends not only on the radial coordinate r (or u) but also on the velocity and the velocity gradient. These characteristics complicate the study of the EoM's topology that gives rise to the different solutions.

Mathematically, singular points are located where the singularity condition is satisfied, i.e.,

$$\frac{\partial}{\partial w'} F(u, w, w') = 0, \quad (48)$$

and these locations form the *locus* of singular points.

At these specific points, in order to have a smooth wind solution between solution branches, a regularity condition must be imposed, namely:

$$\frac{d}{du}F(u, w, w') = \frac{\partial F}{\partial u} + \frac{\partial F}{\partial w}w' = 0 \quad (49)$$

Using the following coordinate transformation:

$$Y = w w' \quad (50)$$

$$Z = w/w', \quad (51)$$

we can now solve Equations (42), (48) and (49), only valid simultaneously at one singular point, obtaining the following set of equations:

$$Y - \frac{1}{Z} + A + 2/u + a_{\text{rot}}^2 u - C' f_1(u, Z) g(u) Z^{-\delta/2} Y^{\alpha-\delta/2} = 0, \quad (52)$$

$$Y - \frac{1}{Z} - C' f_2(u, Z) g(u) Z^{-\delta/2} Y^{\alpha-\delta/2} = 0, \quad (53)$$

$$Y + \frac{1}{Z} - 2Z/u^2 + a_{\text{rot}}^2 Z - C' f_3(u, Z) g(u) Z^{-\delta/2} Y^{\alpha-\delta/2} = 0, \quad (54)$$

derivation details and definitions of $f_1(u, Z)$, $f_2(u, Z)$ and $f_3(u, Z)$ are summarised in Appendix B.

Solving for Y and C' from the set of Equations (52)–(54), we obtain:

$$Y = \frac{1}{Z} + \left(\frac{f_2(u, Z)}{f_1(u, Z) - f_2(u, Z)} \right) \times \left(A + \frac{2}{u} + a_{\text{rot}}^2 u \right) \quad (55)$$

and

$$C'(\dot{M}) = \frac{1}{g f_2} \left(1 - \frac{1}{Y Z} \right) Z^{\delta/2} Y^{1-\alpha+\delta/2} \quad (56)$$

These last two Equations are generalisations of the relations found by [28] (see their Equations (21) and (34) for Y and Equations (21) and (44) for the eigenvalue), but now including the rotational speed of the star.

The Critical Point Function R

The set of Equations (52)–(54) are only valid at the singular point for the unknowns Y_s , C'_s , Z_s and u_s ⁴. Due to the fact that there are only three equations and four unknowns, it is not possible to solve them. Nevertheless, from this set of equations, we can derive the function $R(u, Z)$, defined by:

$$R(u, Z) = -\frac{2}{Z} + \frac{2Z}{u^2} - a_{\text{rot}}^2 Z + f_{123}(u, Z) \left(A + \frac{2}{u} + a_{\text{rot}}^2 u \right) \quad (57)$$

where $f_{123}(u, Z)$ has the following definition:

$$f_{123}(u, Z) = \frac{f_2(u, Z) - f_3(u, Z)}{f_2(u, Z) - f_1(u, Z)} \quad (58)$$

The locus of singular points, u_s , is given by the points which are solutions of the following equation:

$$R(u, Z) = 0. \quad (59)$$

It should be noted that no approximation has been made in the derivation of the above topological equations.

To determine the location of the singular point in the locus of points that satisfies $R(u, Z) = 0$, and therefore determine the values of Y_s , C'_s , Z_s and u_s , we need to set a boundary condition at the stellar surface.

The most used boundary conditions are:

- (i) Set the density at the stellar surface to a specific value,

$$\rho(R_*) = \rho_* \quad (60)$$

Usually this base density is in the range $10^{-8} \text{ g cm}^{-3}$ to $10^{-13} \text{ g cm}^{-3}$. For some examples, see the works of de Araujo and de Freitas Pacheco [47], Friend and MacGregor [48], Madura et al. [49], Curé [50] and Araya et al. [51].

- (ii) Set the optical depth integral to a specific value, i.e.,

$$\tau_* = \int_{R_*}^{\infty} \sigma_E \rho(r) dr = \frac{2}{3}. \quad (61)$$

Employing one of these boundary conditions at the stellar surface plus the regularity condition at the singular point, we can solve from the EoM (Equation (42)) the velocity profile, $w = w(u)$, together with the value of the eigenvalue, C' , and therefore the mass loss rate, \dot{M} .

5. Types of Solutions

We developed a numerical code that discretizes by finite differences the EoM and, using the Newton–Raphson method, iterates to a numerical solution. This code is called HYDWIND and is described in more detail in Curé [50] (see also [52]).

After performing a topological analysis of the EoM, we were able, thanks to HYDWIND, to find the numerical solutions of all three known m-CAK physical solutions: fast, Ω -slow and δ -slow solutions.

5.1. Fast Solution

From the pioneering work of CAK and its improvements from Friend and Abbott [23] and Pauldrach et al. [24], the code HYDWIND is able to obtain the standard solution of the m-CAK theory, hereafter called the fast solution.

To perform our topological analysis, we use a typical O5 V star with the following stellar parameters: $T_{\text{eff}} = 45,000 \text{ K}$, $\log g = 4.0$, $R/R_{\odot} = 12$, and line force parameters $k = 0.124$, $\alpha = 0.64$, and $\delta = 0.07$, with the boundary condition $\tau_* = 2/3$.

The function $R(u, Z)$ is shown in Figure 1 for a non-rotating star ($a_{\text{rot}} = 0$). The plane $R(u, Z) = 0$ is plotted in light grey (right panel) and the intersection of both functions, which corresponds to the locus of singular points, is plotted with a black line. The locus of singular points for the fast solution is the one that starts at $Z \sim 0$ and $u = -1$. The other locus of singular points will be discussed below.

Knowing the topology of the m-CAK model, specifically the locus of singular points, we now solve the EoM for the velocity profile, $v(r)$, or equivalently $w = w(u)$, and the eigenvalue C' , which is proportional to the mass loss rate, \dot{M} . Then, the wind parameters obtained for this model are a terminal velocity (v_{∞}) of 3467 km/s and a mass loss rate (\dot{M}) of $2.456 \times 10^{-6} M_{\odot}/\text{yr}$. Figure 2 shows the velocity profile of this model as a function of $\log(r/R_* - 1)$ (left panel) and as a function of u (right panel). The location of the singular point (r_s) is shown with a red dot, and it is located near the stellar surface ($r_s = 1.029 R_*$ or $u_s = -0.9719$). At this point, the wind velocity is 181.4 km/s, a highly supersonic speed ($a = 24.17 \text{ km/s}$).

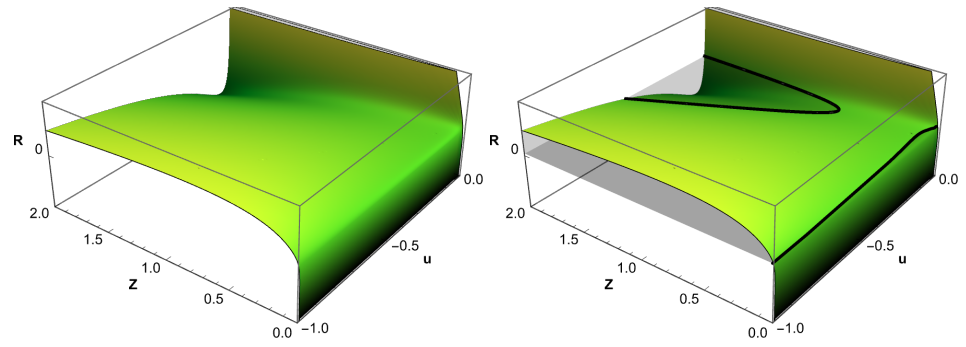


Figure 1. Function $R(u, Z)$ for a typical O5 V star without rotation. The (left panel) shows only the function $R(u, Z)$, while the (right panel) is similar to the (left panel), but the plane $R(u, Z) = 0$ is also plotted in light grey. Furthermore, the intersection of both curves (black solid lines) shows two loci of singular points.

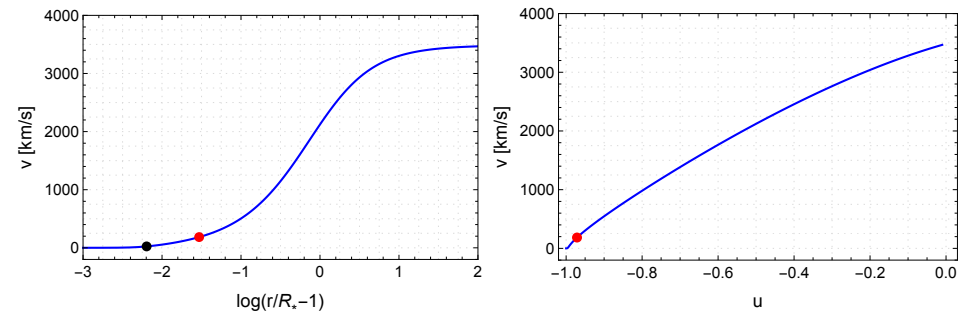


Figure 2. Velocity profile for a typical O5 V star without rotation. The velocity profile is plotted as a function of $\log(r/R_* - 1)$ (left panel) and as a function of u (right panel). The location of the singular point is shown with a red dot, while the sonic point is in black.

This steep velocity gradient is due to the rapid increase in the line force just above the stellar surface, as shown in Figure 3, where the sound speed is reached at $r = 1.006 R_*$ and the maximum of g^{line} is reached at $r = 1.3 R_*$.

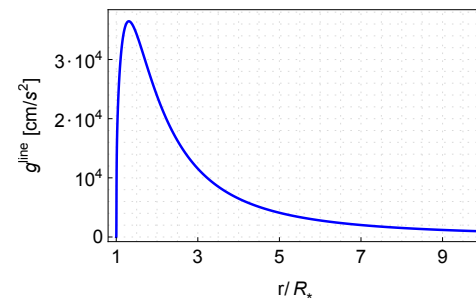


Figure 3. The radiative acceleration, g^{line} , for a typical O5 V star without rotation as function of r/R_* for $r < 10 R_*$.

As previously mentioned, the wind parameters (v_∞ and \dot{M}) must be calculated within the framework of the radiative transport problem. However, to understand the complex non-linear dependence on the wind parameters from the line force parameters, in the following figures, we show how the wind parameters depend on each one of the line force parameters.

Figure 4 shows the dependence of the wind parameters, v_∞ (left panel) and \dot{M} (right panel), as a function of the line force parameter α , using the same stellar parameters and keeping the line force parameters k and δ fixed. There is an increase in the values of both wind parameters as α increases.

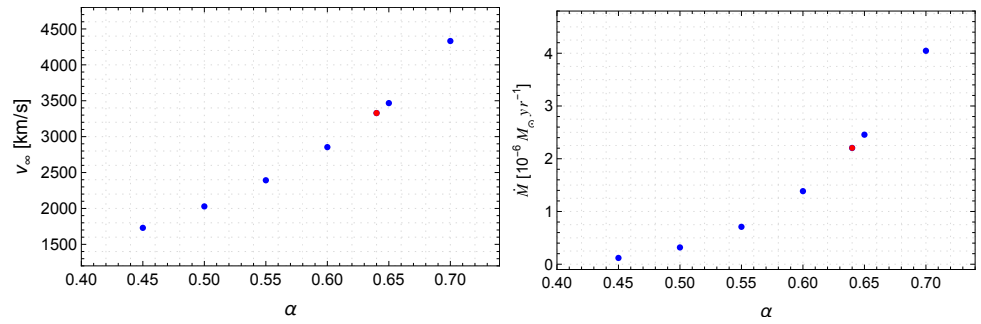


Figure 4. Dependence of the wind parameters as a function of the line force parameter α . Terminal velocity (**left panel**) and mass loss rate (**right panel**). The values obtained for our typical O5 V star without rotation are shown in red.

The dependence of the wind parameters as a function of the line force parameter k is shown in Figure 5. In this case, the wind parameters also increase as k increases. It is clearly seen in Figure 5 that the terminal velocity depends only slightly on the value of k rather than the mass loss rate, which has a significant impact on the value of k [53].

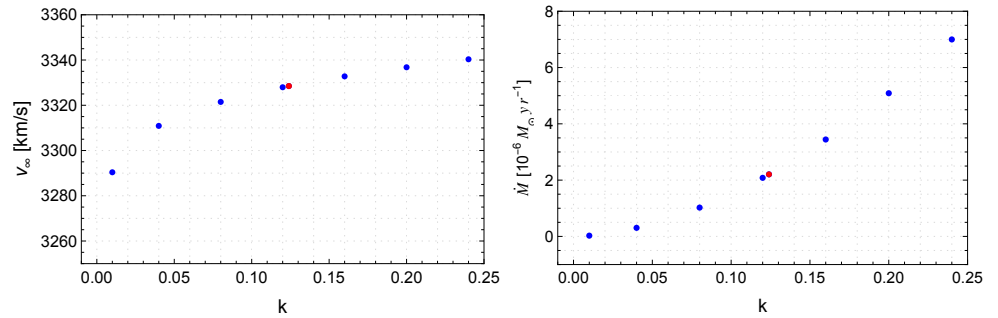


Figure 5. Dependence of the wind parameters as a function of the line force parameter k . Terminal velocity (**left panel**) and mass loss rate (**right panel**). The values obtained for our typical O5 V star without rotation are shown in red.

Finally, the dependence of the wind parameters as a function of the line force parameter δ is shown in Figure 6. We observe that the terminal velocity has a decreasing behaviour when the parameter δ increases, while the mass loss rate can have a decreasing or increasing behaviour. This behaviour depends on the parameter k ; for low values of k , the mass loss rate decreases while δ increases, but for larger values, the behaviour is reversed.

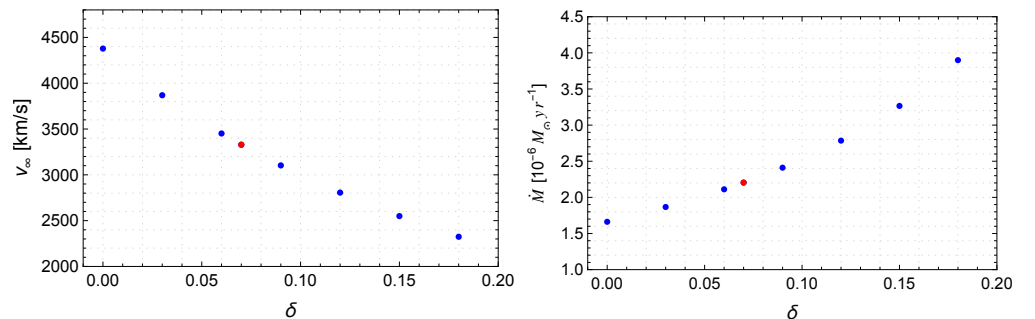


Figure 6. *Cont.*

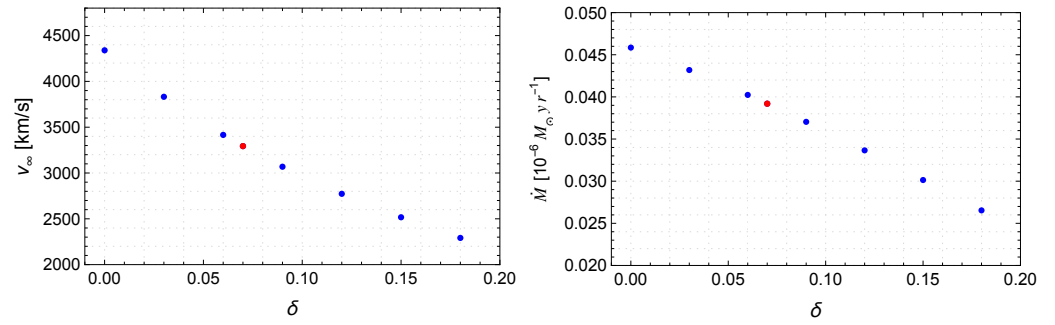


Figure 6. Dependence of the wind parameters as a function of the line force parameter δ . Upper panels are for $k = 0.124$ and lower panels are for $k = 0.0124$. The values obtained for our typical O5 V star without rotation are shown in red.

In the next subsections, we will discuss each of the slow solutions. The combined effects of the line force parameters and the three physical wind solutions are discussed in detail in work by Venero et al. [53].

Overall, the fast solution from the m-CAK theory has been very successful in explaining the terminal velocities and mass loss rates of massive stars (see [8,11–13]).

5.2. Ω -Slow Solution

The original CAK model considered the star point approximation, i.e., all the photons are radially directed over the wind plasma. In that work, CAK only discussed the effect of the finite disc of the star seen by an observer in the wind. Friend and Abbott [23] and Pauldrach et al. [24] implemented the finite disc correction factor and solved the EoM. In both works, they also studied the influence of rotation in the equatorial plane of a rotating star, but they could not obtain solutions for rapidly rotating stars. The reason was found by Curé [50] for values of $\Omega \gtrsim 0.75$, where $\Omega = v_{\text{rot}}/v_{\text{crit}}$. At this value of Ω , the fast solution ceases to exist, and another type of solution is found. This solution, called Ω -slow solution, is characterised by a slower and denser wind in comparison with the fast solution.

It is well known that Be stars are the fastest rotators among stars [54]. Thus, in this section, we will study the topology and the wind solutions for a typical B2.5 V star with the following stellar and line force parameters: $T_{\text{eff}} = 20,000\text{K}$, $\log g = 4.11$, $R/R_\odot = 4.0$, $k = 0.61$, $\alpha = 0.5$ and $\delta = 0.0$. The lower (surface) boundary condition is fixed at $\rho_* = 8.7 \times 10^{-13} \text{g/cm}^3$. In addition, the distortion of the shape of the star caused by its high rotational speed and gravity darkening effects are not considered.

Figure 7 shows the surfaces $R(u, Z)$ for different values of Ω , together with the plane $R(u, Z) = 0$. The intersection of the surfaces $R(u, Z)$ and $R(u, Z) = 0$ (black lines) correspond to the locus of singular points. We clearly observe two different loci of singular points. The fast solution locus can be observed for $\Omega = 0.3$ (upper left panel), $\Omega = 0.5$ (upper right panel) and $\Omega = 0.7$ (lower left panel). For larger rotational rates ($\Omega \gtrsim 0.75$), the fast solution locus lies completely under the plane $R(u, Z) = 0$, as shown in the lower right panel for $\Omega = 0.9$. Thus, the fast solution *does not exist* for large values of Ω .

Figure 8 shows the velocity profiles, $v(u)$, as a function of u for different values of Ω . All these solutions use the same lower boundary condition. This figure shows (left panel) fast solutions in light grey and Ω -slow solutions in coloured lines. The right panel shows only Ω -slow solutions; the location of the singular point is almost independent of Ω . This is a consequence of the shape of the locus curve of singular points (see Figure 7). This locus is located almost at a constant value of u .

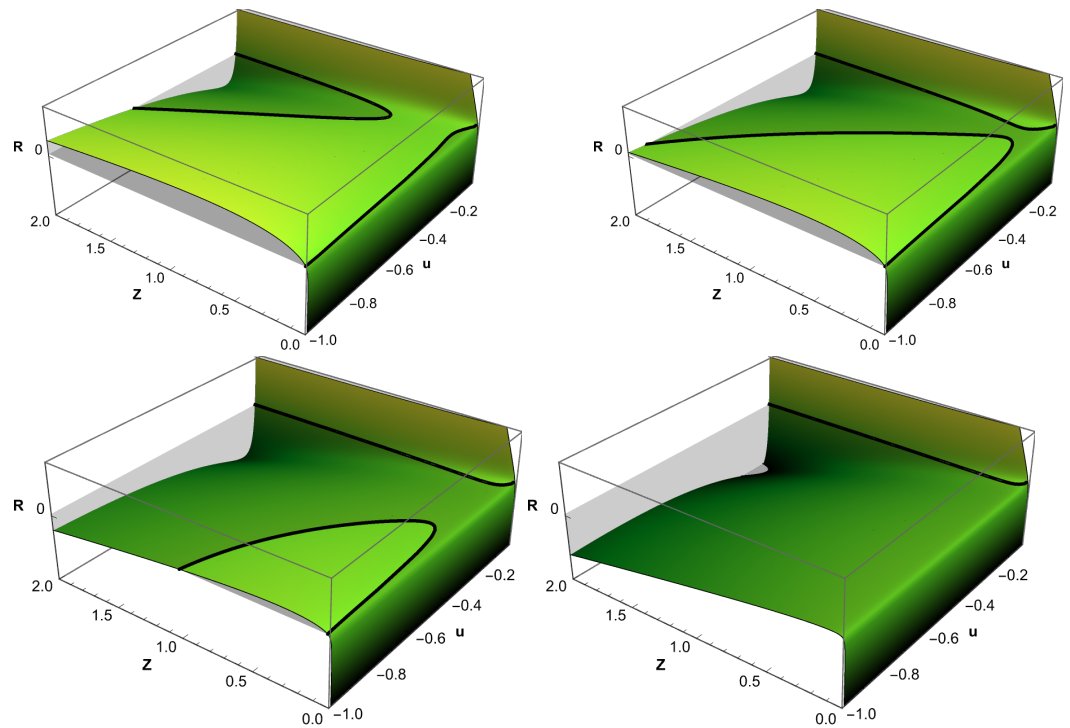


Figure 7. The function $R(u, Z)$ (topology) of the m-CAK theory as function of Ω : $\Omega = 0.3$ (upper left panel), $\Omega = 0.5$ (upper right panel), $\Omega = 0.7$ (lower left panel) and $\Omega = 0.9$ (lower right panel). The plane $R(u, Z) = 0$ is shown in light grey, and its intersection with the surface $R(u, Z)$ (locus of singular points) is plotted with a black line.

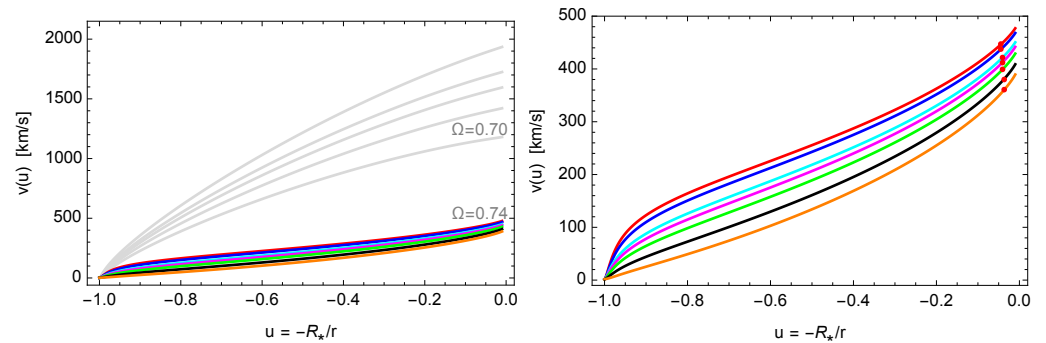


Figure 8. Velocity profiles, $v(u)$, as function of the rotational rate Ω . (**Left panel**): fast solutions ($\Omega \lesssim 0.74$) are plotted in grey lines, while the Ω -slow solutions are in coloured lines: $\Omega = 0.74$ (red line), $\Omega = 0.76$ (blue line), $\Omega = 0.80$ (cyan line), $\Omega = 0.82$ (magenta line), $\Omega = 0.85$ (green line), $\Omega = 0.90$ (black line) and $\Omega = 0.95$ (orange line). (**Right panel**): The same Ω -slow solutions, but zoomed and including the location of the singular points (red dots).

The Ω -slow solutions are only valid in the equatorial plane in this 1D m-CAK model. Notice that this model does not take into account the oblateness and gravity-darkening effects. See Araya et al. [55] for the implementation in the 1D model (equatorial plane) and Cranmer and Owocki [56] for the implementation in the 2D model.

In the equatorial plane, the higher the Ω , the greater the centrifugal force and, consequently, the lower the effective gravity. Therefore, the higher Ω is, the higher the rate of mass loss and, through the continuity equation, the higher the wind density, as shown in Figure 9.

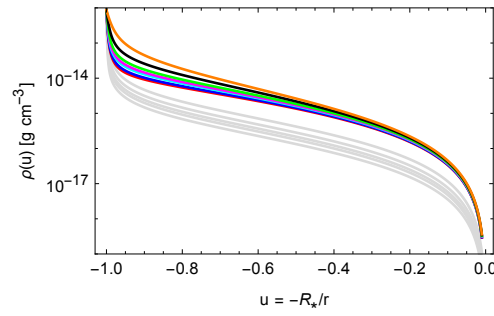


Figure 9. Wind density profiles, $\rho(u)$ (in gr/cm^3) versus u , for fast and Ω -slow solutions. The colour scheme is the same as the one used in Figure 8.

5.3. δ -Slow Solution

The δ -slow solution was found numerically by Curé et al. [27]. This solution, based on the m-CAK theory, describes the wind velocity profile when the ionization-related line force parameter δ takes larger values, $\delta \gtrsim 0.28$. These values are larger than the ones provided by the standard m-CAK solution (see [8] and the references therein). Nevertheless, Puls et al. [42] calculated the value of δ for a pure hydrogen atmosphere, finding a value of $\delta \sim 1/3$. These high values of δ are also found in atmospheres and winds with extremely low metallicities (see [57]).

The δ -slow solution, as well as the Ω -slow solution, are characterized by low velocities. This solution could explain the velocities obtained for late-B and A-type supergiant stars and seems to fit well with the observed anomalous correlation between the terminal and escape velocities found in A supergiant stars [27]. Furthermore, in work by Venero et al. [53] (see their Table 2), a gap of solutions between the fast and the δ -slow solutions for different values of the rotational speed was found in the plane δ - Ω .

To present a topological analysis of this type of solution, we adopt the model T19 from Venero et al. [53]. The stellar and line force parameters are $T_{\text{eff}} = 19,000 \text{ K}$, $\log g = 2.5$, $R/R_{\odot} = 40$, $k = 0.32$ and $\alpha = 0.5$. We use $\tau_* = 2/3$ as a boundary condition at the stellar surface.

In Figure 10, the $R(u, Z)$ function and the plane $R(u, Z) = 0$ are shown for different values of δ . The upper left panel shows the surface $R(u, Z)$ for $\delta = 0.1$. We clearly see that, for this case, the locus of singular points for fast solutions is different from the case of the fast solution shown in Figure 1. Here, this locus is located when $Z \lesssim 0.5$, $\forall u$. The upper right panel shows $R(u, Z)$ for $\delta = 0.12$, where the locus of singular points for fast solutions returns to the behaviour shown in Figure 1. The fast solution is present until $\delta = 0.24$, see the lower left panel. We cannot find fast solutions for slightly larger values of δ until $\delta \sim 0.30$ (lower right panel). For this value of δ , the locus of singular points for fast solutions shifts to slightly larger values of Z for $u \lesssim -1$, and the numerical wind solutions no longer have a singular point in this locus, switching to the other locus of singular points (δ -slow solutions) located at $u \lesssim -0.1$ (or $r \gtrsim 10R_*$).

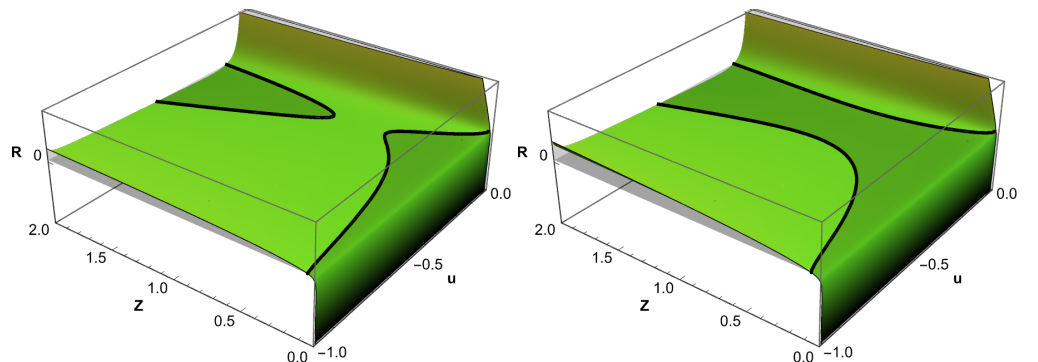


Figure 10. Cont.

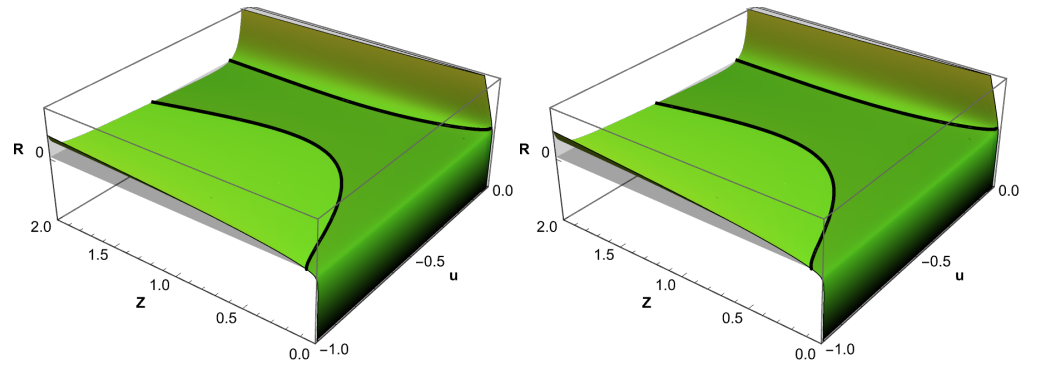


Figure 10. The topological function $R(u, Z)$ of the m-CAK theory as function of δ . (**Upper left panel**): $\delta = 0.1$. (**Upper right panel**): $\delta = 0.12$. (**Lower left panel**): $\delta = 0.24$. (**Lower right panel**): $\delta = 0.3$. The plane $R(u, Z) = 0$ is shown in light grey, and its intersection with the surface $R(u, Z)$ (locus of singular points) is plotted with black lines.

Figure 11 shows the velocity profiles, $v(u)$, as a function of u for different values of δ and the same lower boundary condition. This figure shows (left panel) fast solutions in light grey and δ -slow solutions in coloured lines. The right panel shows only δ -slow solutions. The locus curve of singular points (see Figure 10) is located almost at a constant value of u . Then, the location of the singular point is almost independent of δ , similar to the behaviour of Ω -slow solutions.

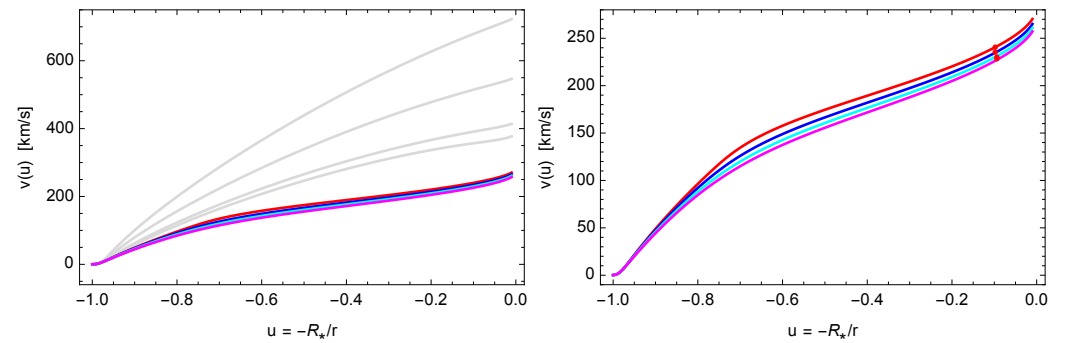


Figure 11. Velocity profiles, $v(u)$, for different values of the line force parameter δ . (**Left panel**): fast solutions are plotted in grey lines for $\delta = 0.0, 0.1, 0.2, 0.24$, while δ -slow solutions are in coloured lines. The red line corresponds to $\delta = 0.3$, the blue line to $\delta = 0.31$, the cyan line to $\delta = 0.32$ and the magenta line to $\delta = 0.33$. The (**right panel**) shows only δ -slow solutions, and the location of the singular points for each solution is shown with a red dot.

5.4. The β -Law Approximation

In the work of Pauldrach et al. [24], after obtaining the numerical solution of the EoM, they assumed a power law approximation to describe the velocity profile only as a function of the radial coordinate r . This approximation is known as the β -law approximation and has the following expression:

$$v(r) = v_{\infty} (1 - R_*/r)^{\beta}, \quad (62)$$

$$= v_{\infty} (1 + u)^{\beta}, \quad (63)$$

where v_{∞} is the terminal velocity and the value of β determines the shape of the velocity profile. In the context of stellar wind diagnostics, these parameters are considered fit parameters that must be determined through spectral line fitting. Usually, the range used for the β parameter is $0.7 \lesssim \beta \lesssim 4$ [11].

Figure 12 shows the velocity profile of the fast solution for the stellar and line force parameters given at the beginning of Section 5.1, together with six different values of β for a β -law velocity profile. From this figure, we can conclude that the fast solution cannot be described properly by a β -law with $\beta > 1.2$.

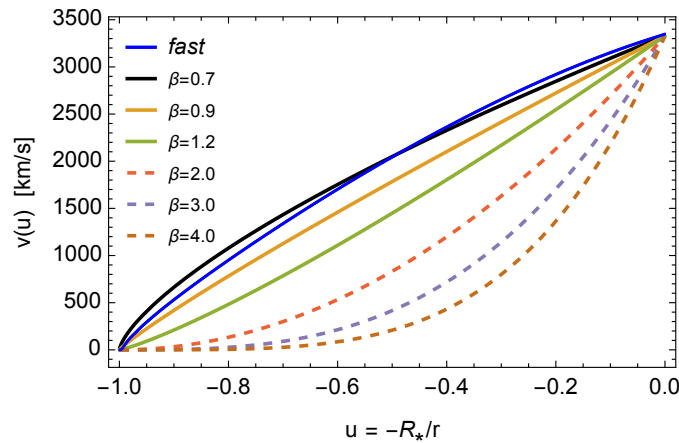


Figure 12. Fast solution velocity profile (solid blue), $v(u)$ vs. u . Six different β -law velocity profiles are also plotted. It is clearly seen that the β -law approximation is a good one for $0.7 \lesssim \beta \lesssim 1.2$. See text for details.

On the other hand, Figure 13 shows the velocity profile for the δ -slow solution for the stellar and line force parameters given at the beginning of Section 5.3, where $\delta = 0.32$. Furthermore, the same β -law profiles of Figure 12 are used, with the proper values of v_∞ for this solution. The same is plotted in Figure 14 for the Ω -slow solution with $\Omega = 0.8$. In the case of the δ -slow solution, the β -law profile cannot fit the m-CAK hydrodynamical solution for any $\beta > 0.7$, while for values around $\beta = 0.7$, the profiles can be considered similar. Finally, from Figure 14, we can definitely conclude that Ω -slow solutions cannot be described properly by any β -law profile.

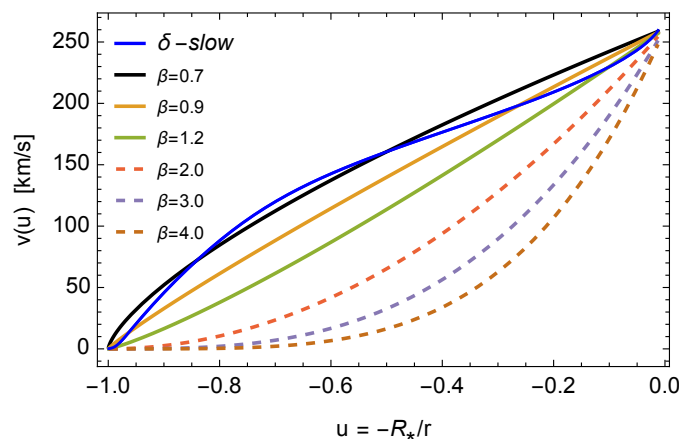


Figure 13. δ -slow solution velocity profile (solid blue), $v(u)$ vs. u . Six different β -law velocity profiles are also plotted. For values around $\beta = 0.7$, the profiles can be considered similar, but it can be clearly concluded that for $\beta > 0.7$, the β -law profile cannot fit the m-CAK hydrodynamical δ -slow solution.

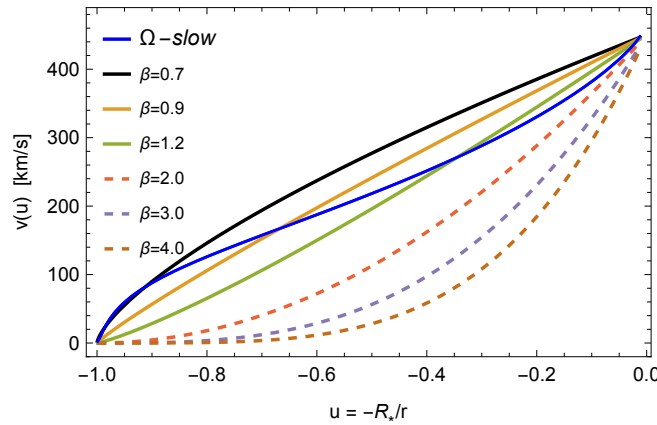


Figure 14. Ω -slow solution velocity profile (solid blue), $v(u)$ vs. u . Six different β -law velocity profiles are also plotted. It can be clearly concluded that no β -law profile can fit the m-CAK hydrodynamical Ω -slow solution.

6. Analytical Wind Solutions

Using an analytical expression to represent the radiation force and solve the equation of motion analytically offers numerous advantages over the numerical integration of the EoM. These formulae can be used in all cases where good first estimates are needed; for example, it gives the advantage of solving the radiative transfer problem for moving media in an easier way.

Kudritzki et al. [28] were some of the first to develop analytical solutions for radiation-driven winds considering the finite disc correction factor in the line force. Based on these solutions, they provided approximated analytical expressions for the terminal velocity and the mass loss rate in terms of the stellar parameters (L , M_* and R_*), the line force parameters (k , α and δ) and the free parameter β from the β -law (they adopted $\beta = 1.0$ for their results).

Other authors have tried to simplify the complicated numerical treatment from the theory. Villata [58], with the purpose of simplifying the integration of the EoM, derived an approximated expression for the line acceleration term, which depends only on the radial coordinate. Müller and Vink [59] presented an analytical expression for the velocity field using a parameterized description for the line acceleration that (as in Villata [58]) also depends on the radial coordinate. These line acceleration expressions do not depend on the velocity or the velocity gradient, as the standard m-CAK description does. Araya et al. [60] proposed to achieve a complete analytical description of the 1D hydrodynamical solution for radiation-driven winds in the fast regime by gathering the advantages of both previous approximations (the use of known parameters and the LambertW function). In addition, Araya et al. [61] developed an analytical solution for the δ -slow regime. To date, no approximation using the LambertW function has been performed for the Ω -slow regime, we expect to do this in the future.

In the following sections, we describe the results and methodology used to analytically solve the equation of motion for fast and δ -slow regimes.

6.1. Solution of the Dimensionless Equation of Motion

In this section, we recapitulated the methodology described by Müller and Vink [59] to obtain the dimensionless equation of motion.

In a dimensionless form, the momentum equation can be expressed as follows,

$$\hat{v} \frac{d\hat{v}}{d\hat{r}} = -\frac{\hat{v}_{\text{crit}}^2}{\hat{r}^2} + \delta^{\text{line}} - \frac{1}{\rho} \frac{d\rho}{d\hat{r}}, \quad (64)$$

where \hat{r} is a dimensionless radial coordinate $\hat{r} = r/R_*$ and the dimensionless velocities (in units of the isothermal sound speed a) are:

$$\hat{v} = \frac{v}{a} \quad \text{and} \quad \hat{v}_{\text{crit}} = \frac{v_{\text{esc}}}{a\sqrt{2}}, \quad (65)$$

where v_{crit} is the rotational break-up velocity in the case of a rotating star. It is usually determined by dividing the effective escape velocity, v_{esc} , by a factor of $\sqrt{2}$. Similarly, a dimensionless line acceleration can be written as follows:

$$\hat{g}^{\text{line}} = \frac{R_*}{a^2} g^{\text{line}}. \quad (66)$$

Using the continuity equation and the equation of state of an ideal gas, the dimensionless equation of motion reads as follows:

$$\left(\hat{v} - \frac{1}{\hat{v}} \right) \frac{d\hat{v}}{d\hat{r}} = -\frac{\hat{v}_{\text{crit}}^2}{\hat{r}^2} + \frac{2}{\hat{r}} + \hat{g}^{\text{line}}(\hat{r}). \quad (67)$$

Lastly, a 1D velocity profile is derived analytically in terms of the LambertW function [62–64]. See Müller and Vink [59] for a detailed description of the methodology used to arrive at this solution. This analytical solution is expressed as follows:

$$\hat{v}(\hat{r}) = \sqrt{-W_j(x(\hat{r}))}, \quad (68)$$

where

$$x(\hat{r}) = -\left(\frac{\hat{r}_c}{\hat{r}}\right)^4 \exp\left[-2\hat{v}_{\text{crit}}^2\left(\frac{1}{\hat{r}} - \frac{1}{\hat{r}_c}\right) - 2\int_{\hat{r}_c}^{\hat{r}} \hat{g}^{\text{line}}(\hat{r})d\hat{r} - 1\right]. \quad (69)$$

In the last equation appears the parameter \hat{r}_c , which represents the position of the sonic (or critical) point.

Furthermore, the LambertW function (W_j) has only two real branches, indicated by the sub-index j , where $j = 0$ or -1 . These two branches coincide at the sonic point, \hat{r}_c , i.e.,

$$j = \begin{cases} 0 & \text{for } 1 \leq \hat{r} \leq \hat{r}_c \\ -1 & \text{for } \hat{r} > \hat{r}_c \end{cases} \quad (70)$$

A regularity condition must be imposed, as in the m-CAK case, since the LHS of the equation of motion (Equation (67)) vanishes at $\hat{v} = 1$ (singularity condition in the CAK formalism). This is equivalent to ensuring that the RHS of Equation (67) vanishes at $\hat{r} = \hat{r}_c$. Therefore,

$$-\frac{\hat{v}_{\text{crit}}^2}{\hat{r}_c^2} + \frac{2}{\hat{r}_c} + \hat{g}^{\text{line}}(\hat{r}_c) = 0, \quad (71)$$

and \hat{r}_c is obtained by solving this last equation. Finally, the velocity profile is derived using the function $x(\hat{r})$, Equation (69), in Equation (68).

6.2. The Fast Regime

Kudritzki et al. [28] analytical study of radiation-driven stellar winds allowed Villata [58] to derive an approximate expression for the line acceleration term. In this case, the line acceleration is only dependent on the radial coordinate, and it reads as follows:

$$g_{\text{V92}}^{\text{line}}(\hat{r}) = \frac{G M_* (1 - \Gamma_e)}{R_*^2 \hat{r}^2} A(\alpha, \beta, \delta) \left(1 - \frac{1}{\hat{r}}\right)^{\alpha(2.2\beta-1)}, \quad (72)$$

with

$$A(\alpha, \beta, \delta) = \frac{(1.76\beta)^\alpha}{1-\alpha} [10^{-\delta}(1+\alpha)]^{1/(1-\alpha)} \left[1 + \left(\frac{2}{\alpha}\left\{1 - [10^{-\delta}(1+\alpha)]^{1/(\alpha-1)}\right\}\right)^{1/2}\right]^\alpha. \quad (73)$$

According to Kudritzki et al. [65], the exponent β can be calculated based on the force multiplier parameters and the escape velocity, v_{esc} :

$$\beta = 0.95\alpha + \frac{0.008}{\delta} + \frac{0.032 v_{\text{esc}}}{500}, \quad (74)$$

with v_{esc} in km/s.

Then, using Equation (72) in its dimensionless form (Equation (66)) and inserting it into the dimensionless equation of motion (Equation (67)) yields:

$$\left(\hat{v} - \frac{1}{\hat{v}}\right) \frac{d\hat{v}}{d\hat{r}} = -\frac{\hat{v}_{\text{crit}}^2}{\hat{r}^2} + \frac{2}{\hat{r}} + \frac{1}{a^2} \frac{GM_*(1 - \Gamma_e)}{R_* \hat{r}^2} A(\alpha, \beta, \delta) \left(1 - \frac{1}{\hat{r}}\right)^{\gamma_v}, \quad (75)$$

with $\gamma_v = \alpha(2.2\beta - 1)$.

Based on Villata [58] approximation of the line acceleration, this differential equation can be viewed as a solar-like differential equation of motion. Hence, the singular point is the sonic point. Additionally, Villata [58] equation of motion does not have eigenvalues, which means it does not depend explicitly on the star's mass loss rate.

Using a standard numerical integration method, Villata [58] solved the equation of motion and obtained terminal velocities that were within 3–4 % of those computed by Pauldrach et al. [24] and Kudritzki et al. [65].

A parametrized description of the line acceleration was presented years later by Müller and Vink [59] that is dependent on the radial coordinate (similar to Villata [58]). The line acceleration in Müller and Vink [59] was determined using Monte Carlo multi-line radiative transfer calculations [66,67] and a β law. Following this, the line acceleration was fitted using the following formula:

$$\hat{g}_{\text{MV08}}^{\text{line}}(\hat{r}) = \frac{\hat{g}_0}{\hat{r}^{1+\delta_1}} \left(1 - \frac{\hat{r}_0}{\hat{r}^{\delta_1}}\right)^{\gamma}, \quad (76)$$

where \hat{g}_0 , δ_1 , \hat{r}_0 and γ are the acceleration line parameters.

Then, the solution of the equation of motion, based on their methodology and line acceleration, is:

$$\hat{v}(\hat{r}) = \sqrt{-W_j(x(\hat{r}))}, \quad (77)$$

with

$$x(\hat{r}) = -\left(\frac{\hat{r}_c}{\hat{r}}\right)^4 \exp\left[-2\hat{v}_{\text{crit}}^2\left(\frac{1}{\hat{r}} - \frac{1}{\hat{r}_c}\right) - \frac{2}{\hat{r}_0 \delta_1 (1 + \gamma)} \left(\left(1 - \frac{\hat{r}_0}{\hat{r}^{\delta_1}}\right)^{1+\gamma} - \left(1 - \frac{\hat{r}_0}{\hat{r}_c^{\delta_1}}\right)^{1+\gamma} \right) - 1\right]. \quad (78)$$

As a result of the approximations described above, the velocity profile can be represented analytically, greatly simplifying the solution of the equation of motion.

Furthermore, it is relevant to note that each of the mentioned approximations has its own advantages and disadvantages. Even though Villata's approximation of the radiation force is general and can directly be applied to describe any massive star's wind, the momentum equation still needs to be solved numerically. With Müller and Vink [59] approximation, the equation of motion can be analytically solved based on the \hat{g}_0 , δ_1 , \hat{r}_0 and γ parameters of the star. Nevertheless, it is still necessary to perform Monte Carlo multi-line radiative transfer calculations in order to determine these parameters.

This methodology to solve the equation of motion was revisited by Araya et al. [60] in order to derive a fully analytical expression combining Villata [58] expression of the equation of motion with the methodology developed by Müller and Vink [59].

This analytical solution is,

$$\hat{v}(\hat{r}) = \sqrt{-W_j(x(\hat{r}))}, \quad (79)$$

with

$$x(\hat{r}) = -\left(\frac{\hat{r}_c}{\hat{r}}\right)^4 \exp\left[-2\hat{v}_{\text{crit}}^2\left(\frac{1}{\hat{r}} - \frac{1}{\hat{r}_c}\right) - 2\left(I_{\delta_{V92}}^{\text{line}}(\hat{r}) - I_{\delta_{V92}}^{\text{line}}(\hat{r}_c)\right) - 1\right], \quad (80)$$

where

$$I_{\delta_{V92}}^{\text{line}}(\hat{r}) = \left(10^{-\delta}(1+\alpha)\right)^{\frac{1}{1-\alpha}} \left(1 + \sqrt{2} \sqrt{-\frac{(10^{-\delta}(1+\alpha)-1)^{\frac{1}{\alpha-1}}}{\alpha}}\right)^{\alpha} \\ \times (1.76\beta)^{\alpha} G M_* \left(\frac{\hat{r}-1}{\hat{r}}\right)^{1+\gamma_v} \frac{\Gamma-1}{(a^2[\alpha-1](1+\gamma_v) R_*)}. \quad (81)$$

As was mentioned in the previous section, \hat{r}_c can be obtained numerically, making the RHS of Equation (75) equal to zero. In order to obtain the terminal velocity in a simpler way, we can use the average value of \hat{r}_c ($\bar{\hat{r}}_c = 1.0026$) obtained by Araya et al. [60]. Note that this value can be used only in the supersonic region.

Equation (79) has the advantage that it is based not only on the LambertW function, but also on stellar parameters and the line force parameters. For a wide range of spectral types, stellar and force multiplier parameters are given (see, e.g., [8,10,22,24,41,44]).

By comparing the analytical solution to the 1D hydrodynamic code HYDWIND, the accuracy of the analytical solution can be tested. Figure 15 compares the results obtained with our analytical approximation to those obtained with the hydrodynamics for four stars taken from Araya et al. [60]. Both solutions have similar behaviour. However, as shown by Araya et al. [60], the analytical approximation close to the stellar surface (subsonic region) is not good enough. In the same way, Figure 16 compares the numerical and analytical velocity profiles near to the stellar surface for ϵ Ori.

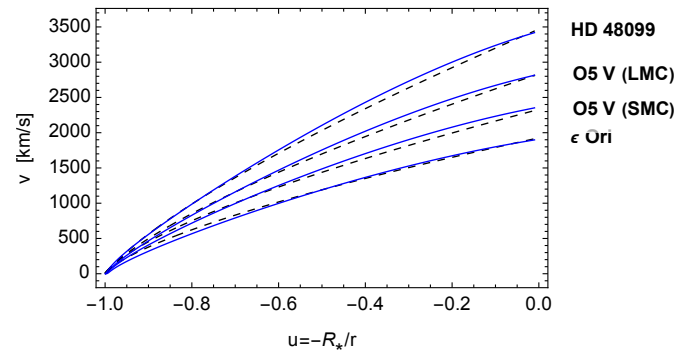


Figure 15. Velocity profiles as a function of the inverse radial coordinate $u = -R_*/r = -1/\hat{r}$ for four models. The hydrodynamic results from HYDWIND are shown in solid blue lines and the analytical solutions are shown by dashed lines. The stellar and line force parameters for the models are given in Araya et al. [60].

There is a limitation to this analytical expression when the line force parameter δ exceeds about 0.3. This is due to the complexity of a term in the proposed line acceleration expression. To obtain an expression with real values, high values of δ would require high values of α . However, such kind of α values would be totally unphysical ($\alpha > 1$). As an illustration of the dependence of this expression on the parameters α and δ , Figure 17 shows the domain of the complex and real regions when this expression is evaluated to the given line acceleration term.

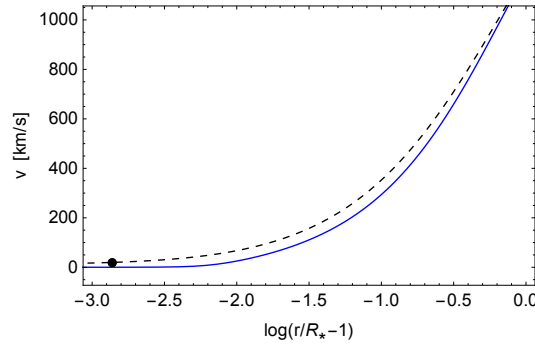


Figure 16. Velocity profiles of ϵ Ori as a function of $\log(r/R_* - 1)$ in a region near to the stellar surface. The solid blue line shows the numerical hydrodynamic result and the analytical solution is shown by a dashed line. The dot symbol indicates the position of the sonic (or critical) point. The difference between both curves is around one thermal speed.

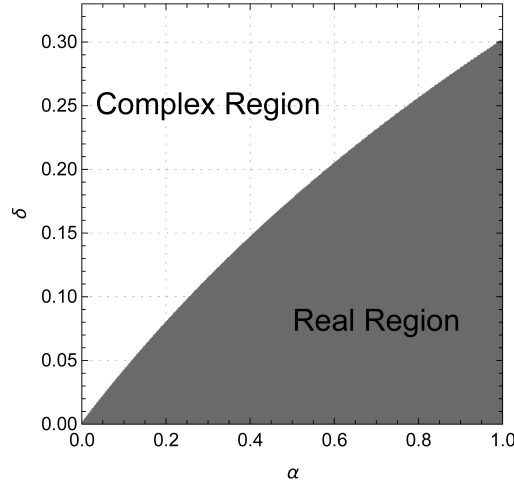


Figure 17. Real and complex regions where the line acceleration expression given by Villata [58] can be found. These regions are delimited by the values of the line force parameters α and δ .

6.3. The δ -Slow Regime

Considering the results obtained when using an approximate description of the wind velocity for the δ -slow case, Araya et al. [61] modified the function of the line acceleration given by Müller and Vink [59] to better describe of δ -slow wind.

As a result, the proposed line acceleration is:

$$g^{\text{line}}(\hat{r}) = \frac{\hat{g}_0}{\hat{r}^{1+\delta_1}} \left(1 - \frac{1}{\hat{r}^{\delta_2}} \right)^\gamma, \quad (82)$$

where \hat{g}_0 , δ_1 , δ_2 and γ are the new set of line acceleration parameters.

It is notable that the δ_2 parameter, which has been incorporated into this new expression, provides a much better agreement with the numerical line acceleration obtained from the m-CAK model in the δ -slow regime compared with the one from Müller and Vink [59].

Based on this new definition of the radiation force, the new dimensionless equation of motion reads:

$$\left(\hat{v} - \frac{1}{\hat{v}} \right) \frac{d\hat{v}}{d\hat{r}} = -\frac{\hat{v}_{\text{crit}}^2}{\hat{r}^2} + \frac{2}{\hat{r}} + \frac{\hat{g}_0}{\hat{r}^{1+\delta_1}} \left(1 - \frac{1}{\hat{r}^{\delta_2}} \right)^\gamma. \quad (83)$$

The LambertW function is used to solve the equation of motion, Equation (83), following the same methodology developed by Müller and Vink [59],

$$\hat{v}(\hat{r}) = \sqrt{-W_j(x(\hat{r}))}, \quad (84)$$

with

$$x(\hat{r}) = -\left(\frac{\hat{r}_c}{\hat{r}}\right)^4 \exp\left[-2\hat{v}_{\text{crit}}^2\left(\frac{1}{\hat{r}} - \frac{1}{\hat{r}_c}\right) - 2\left(I_{\hat{g}^{\text{line}}}(\hat{r}) - I_{\hat{g}^{\text{line}}}(\hat{r}_c)\right) - 1\right],$$

where

$$I_{\hat{g}^{\text{line}}} = \int \hat{g}^{\text{line}}(\hat{r}) d\hat{r} = -\frac{g_0 \hat{r}^{-\delta_1} {}_2F_1\left[-\gamma, \frac{\delta_1}{\delta_2}, 1 + \frac{\delta_1}{\delta_2}, \hat{r}^{-\delta_2}\right]}{\delta_1}, \quad (85)$$

and ${}_2F_1$ is the Gauss Hypergeometric function. The critical (or sonic) point, \hat{r}_c is obtained numerically, making the RHS of Equation (83) equal to zero.

Ultimately, this expression for the velocity profile is in quite satisfactory agreement with the numerical solution from HYDWIN.

As described in Araya et al. [60], a relationship was established between the Müller and Vink [59] line force parameters (g_0 , δ_1 , r_0 and γ) and the stellar and m-CAK line force parameters. In addition to being easy to use, this relationship provides a straightforward and versatile method of calculating velocity profiles analytically for a wide range of spectral types, since both stellar and m-CAK line force parameters are available (see [8,10,22,24,41,44]).

A similar relationship can be derived for the δ -slow regime using m-CAK hydrodynamic models, that is, creating a grid of HYDWIN models for δ -slow solutions. These models are then analysed using a multivariate multiple regression analysis (MMR [68,69]).

To develop this hydrodynamic grid, the stellar radius is calculated from M_{bol} for each pair of stellar parameters (T_{eff} and $\log g$) by using the flux weighted gravity–luminosity relationship [70,71]. Additionally, a total of 20 stellar radius values were added (ranging from $5 R_{\odot}$ to $100 R_{\odot}$ in steps of $5 R_{\odot}$). The surface gravities are in the range of $\log g = 2.7$ down to about 90% of Eddington’s limit in steps of 0.15 dex. The effective temperatures are between 9 000 K and 19, 500 K in steps of 500 K. The range of this grid has been chosen to cover the region of the $T_{\text{eff}}\text{--}\log g$ diagram that contains B- and A-type supergiants. In Table 1, the m-CAK line force parameters for each set of (T_{eff} , $\log g$) values are listed. For the purpose of obtaining δ -slow solutions, only high values of δ are considered. For the $T_{\text{eff}}\text{--}\log g$ plane (see Figure 18), we show in blue dots all converged models.

Table 1. m-CAK line force parameter ranges for the grid of models.

Parameter	Range
α	0.45–0.69 (step size of 0.02)
k	0.05–1.00 (step size of 0.05)
δ	0.26–0.35 (step size of 0.01)

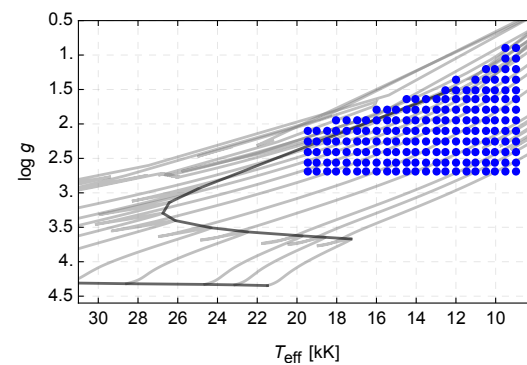


Figure 18. Hydrodynamic models in the $T_{\text{eff}}\text{--}\log g$ plane. Blue dots represent the converged solutions. Grey solid lines are the evolutionary tracks for stars of $7M_{\odot}$ to $60M_{\odot}$ without rotation [72], and black lines represent the zero-age main sequence (ZAMS) and the terminal age main sequence (TAMS).

In order to obtain the new line acceleration parameters (\hat{g}_0 , δ_1 , δ_2 and γ) for each model, the m-CAK line acceleration was fitted, using Least Squares, with the proposed line acceleration expression (Equation (82)). Then, an MMR is applied to the grid of models in order to derive the relationship between the new line acceleration parameters (\hat{g}_0 , δ_1 , δ_2 and γ) and stellar (T_{eff} , $\log g$ and R_*/R_\odot) and m-CAK line force parameters (k , α and δ). The estimated parameters are:

$$\begin{aligned} \hat{g}_0^{0.27} = & -4.548 - 1.890 \times 10^{-4} T_{\text{eff}} + \\ & 4.393 \log g + 3.026 \times 10^{-2} R_*/R_\odot - \\ & 4.802 \times 10^{-3} k + 3.781 \alpha - 3.212 \delta, \end{aligned} \quad (86)$$

$$\begin{aligned} (\delta_1 + 1)^{5.3} = & -4.623 - 3.743 \times 10^{-4} T_{\text{eff}} + \\ & 1.489 \times 10^1 \log g + 1.148 \times 10^{-1} R_*/R_\odot + \\ & 2.415 k + 9.553 \times 10^1 \alpha - 1.320 \times 10^2 \delta, \end{aligned} \quad (87)$$

$$\begin{aligned} \delta_2^{0.45} = & 5.359 + 8.262 \times 10^{-5} T_{\text{eff}} - \\ & 1.327 \log g - 8.327 \times 10^{-3} R_*/R_\odot + \\ & 2.181 \times 10^{-1} k + 9.618 \times 10^{-1} \alpha - 2.296 \delta \end{aligned} \quad (88)$$

and

$$\begin{aligned} (\gamma + 1)^{-3.56} = & -1.031 + 7.254 \times 10^{-6} T_{\text{eff}} + \\ & 2.994 \times 10^{-1} \log g + 3.097 \times 10^{-3} R_*/R_\odot + \\ & 1.836 \times 10^{-1} k - 4.828 \times 10^{-1} \alpha + 1.254 \delta, \end{aligned} \quad (89)$$

After the estimated values for each dependent variable ($\hat{g}_0^{0.27}$, $(\delta_1 + 1)^{5.3}$ and $\delta_2^{0.45}$, $(\gamma + 1)^{-3.56}$) are obtained they are transformed into \hat{g}_0 , δ_1 , δ_2 and γ through their respective inverse functions. Finally, we can use these parameters in Equation (84) to calculate the velocity profile.

The velocity profiles obtained via HYDWIN code and the analytical solution are shown in Figure 19 for one model with a δ -slow solution. The model is taken from Curé et al. [27].

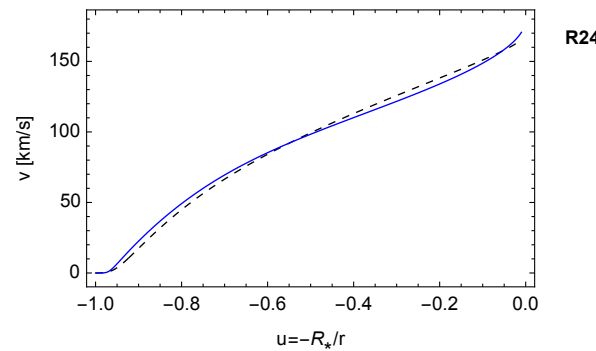


Figure 19. Velocity profiles as a function of the inverse radial coordinate $u = -R_*/r = -1/\hat{r}$ for the model R24 from Curé et al. [27]. The hydrodynamic result from HYDWIN is shown in the solid blue line and the analytical solution is a dashed black line.

Remember, however, that this relationship holds only for δ -slow solutions, especially for values of δ between 0.29 and 0.35. In addition, considering the number of converged models in the grid, the authors recommend using this expression for values of α between 0.45 and 0.55.

Finally, it is important to remark that both analytical solutions for the velocity profile, fast and δ -slow, do depend only on the stellar (T_{eff} , $\log g$ and R_*/R_\odot) and m-CAK line force parameters (k , α and δ). Regarding the mass loss rate, Villata [58] proposed an expression to obtain it (in terms of the stellar and m-CAK parameters) following the approximations given by Kudritzki et al. [28]. Furthermore, Araya et al. [61], in the appendix, proposed a method to obtain the mass loss based on Curé [50].

7. Summary and Discussion

Observations in recent decades have shown that the basic wind parameters behave as predicted by theory. This fundamental agreement between observations and theory provides strong evidence that the winds from massive stars are driven by radiation pressure. This has given m-CAK theory a well-established status in the massive star community. However, several issues are contentious and still unclear, such as the calibration of the wind momentum–luminosity relationship (WLR) [73], discs of Be stars, wind parameter determination and the applicability of the so-called slow wind solutions, among others. All these issues are the focus of massive stars research.

This review is focused on the theoretical and numerical research of wind hydrodynamics of massive stars based on the m-CAK theory, with particular emphasis on its topology and hydrodynamic solutions.

We presented a topological analysis of the one-dimensional m-CAK hydrodynamic model and its three known hydrodynamic solutions, the fast, Ω -slow and δ -slow solutions. From a topological point of view, slow solutions are obtained from a new branch of solutions with a locus of singular points far from the stellar surface, unlike fast solutions with a family of singular points near the stellar surface.

We continued analyzing the dependence of the line force parameters (k , α and δ) with the wind parameters (mass loss rate and terminal velocity) in order to understand the complex non-linear dependence between these parameters. In the case of α , there is an increase in both wind parameters as this parameter increases. This behaviour is similar to the k parameter, but the dependence is very slight for terminal velocity, while the mass loss rate has a significant impact. For the δ parameter, the terminal velocity has a decreasing behaviour when this parameter increases, while the mass loss rate can have a decreasing or increasing behaviour, which depends on the parameter k . When k is low, mass loss rates decrease while δ increases, whereas when k is large, the opposite occurs.

In addition, we compared the β -law with the hydrodynamic solutions. We concluded that the fast solution could not be adequately described by a β -law with $\beta > 1.2$, while the δ -slow solution cannot be described by any β -law.

Furthermore, we presented two analytical expressions for the solution of line-driven winds in terms of the stellar and line force parameters. The expressions are addressed to obtain the fast and δ -slow velocity regimes in a simple way. Both solutions are based on the LambertW function and an approximative expression for the wind line acceleration as a function of the radial distance. The importance of an analytical solution lies in its simplicity in studying the properties of the wind instead of solving complex hydrodynamic equations. In addition, these analytical expressions can be used in radiative transfer or stellar evolution codes (see, e.g., [74]).

Concerning the applicability of the slow solutions, in the case of the Ω -slow solution, their behaviour suggests that it can play a paramount role in the ejection of material to the equatorial circumstellar environment of Be and B[e] stars. Be stars are a unique set of massive stars whose main distinguishing characteristics are a rapid rotation and the presence of a dense, gaseous circumstellar disc orbiting in a quasi-Keplerian fashion. There is a long-standing problem in understanding the formation of discs in Be stars; this is one of the major areas of ongoing research in Be stars. The gaseous discs are not remnants of the objects' protostellar environments, nor are they formed through the accretion of material [54,75]. On the contrary, the equatorial gas consists of a decretion disc formed from a material originating from the central star.

As was stated above, attempts to solve this problem have been made without much success, for example, the link between the line-driven winds and these discs, called the wind-compressed discs [76], but the work of Owocki et al. [77] was the first to show this is not a viable mechanism for rapidly rotating stars due to the non-radial line force components. The most accepted model to successfully reproduce many Be star observations is the viscous decretion disc (VDD) model, developed by Lee et al. [78] and examined by Okazaki [79], Bjorkman and Carciofi [25], Kr̥iřka et al. [80] and Curé et al. [81]. Currently, how that material is ejected into the equatorial plane and how sufficient angular momentum is transferred to the disc to maintain quasi-Keplerian rotation are among the primary unresolved questions currently driving classical Be star research.

Araya et al. [55] studied the Ω -slow wind solution and its relation with the discs of Be stars. Overall, this work is an extension to the study performed by Silaj et al. [82], where they precisely investigated if the density distribution provided by the Ω -slow wind solution could adequately describe the physical conditions to form a dense disc in Keplerian rotation via angular momentum transfer. They considered a two-component wind model, i.e., a fast, thin wind in the polar latitudes and a Ω -slow, dense wind in the equatorial regions. Based on the equatorial density distributions, H α line profiles were generated and compared with an ad hoc emission profile, which agreed with the observations. In addition, their calculations assumed three different scenarios related to the shape (oblate correction factor) and the star's brightness (gravity darkening). Finally, they found that under certain conditions (related to the line force parameter of the wind), a significant H α line profile could be produced, and it may be that the line-driven winds through the Ω -slow solution have an essential role in the disc formation of Be stars.

In addition, Araya et al. [51] studied the zone where the classical m-CAK fast solution ceases to exist, and the Ω -slow solution emerges at rapid rotational speeds. This study used two hydrodynamic codes with time-dependent and stationary approaches. They found that both solutions can co-exist in this transition region, which depends exclusively on the initial conditions. In addition, they performed base density wind perturbations to test the stability of the solution within the co-existence region. A switch of the solution was found under certain perturbation conditions. The results are explained by a possible role in the ejection of extra material into the equatorial plane of pulsation modes, where the Ω -slow solution can play an important role.

A current weakness of this m-CAK model is that it does not consider the role of viscosity and its influence on angular momentum transport. This mechanism might explain the formation of a Keplerian disc.

On the other hand, the δ -slow solution is promising to explain the discrepancies of the wind parameters between observations and theory in late B- and A-type supergiant stars. According to the findings of Venero et al. [53], these suggest that the terminal velocity of early and mid-B supergiants agrees with the results seen from fast outflowing winds. In contrast, the results obtained for late B supergiants and, mainly, those obtained for early A supergiants, agree with the results achieved for δ -slow stationary outflowing wind regimes. Then, the δ -slow solution enables us to describe the global features of the wind quite well, such as mass loss rates and terminal velocities of moderately and slowly rotating B supergiants.

Conversely, Venero et al. [53] stated that the δ -slow solution seems not to be present in stars with $T_{\text{eff}} > 21,000$ K. This restricts the possibility of a switch between fast and slow regimes at such temperatures. Consequently, this would be a physical explanation for why an empirical bi-stability jump can be observed around 21,000 K in B supergiants [83]. From a theoretical perspective, a velocity jump has also been found using Monte Carlo modelling and the co-moving frame method (see, e.g., [13,84,85]).

In addition, it is generally accepted that most O and early B-type stars can be adequately modelled with a β velocity law with $0.7 \lesssim \beta \lesssim 1.2$. However, supergiants A and B exhibit β values that tend towards higher values, often $\beta \geq 2$ (see, e.g., [86–90]). Venero et al. 2023 (in preparation) propose that δ -slow solutions might explain these winds. They show

that the δ -slow regime could adequately fit the H α line profile of B supergiants with the same accuracy as that obtained using a β -law with $\beta \geq 2$, but now with a hydrodynamic explanation of the velocity profile used.

The investigations carried out in the latest works inspired us to go deeper into the possible role of slow wind solutions with respect to the unresolved questions related to massive stars. In view of our results, we are encouraged to develop this line of research further. In the case of the Ω -slow solution and its link to Be stars, or possibly to B[e] stars, it would require 2D/3D models for a better understanding to take into account non-radial forces, the effects of stellar distortion and gravity darkening. These considerations could change, in turn, the nature of the Ω -slow solution or the behaviour regarding the co-existence of solutions and a switch between them.

The δ -slow solution could play an essential role in understanding the winds of B- and A-type supergiants. Moreover, this solution is expected to solve the disagreement between the observations and theory for these stars and, in this way, calibrate the wind momentum–luminosity relationship.

As we mentioned previously, in the standard procedure for finding stellar and wind parameters, the β -law (β and v_∞) and the mass loss rate (\dot{M}) are three ‘free’ input parameters in radiative transfer codes, comparing synthetic spectra with the observed spectra of a star. The β law comes from an approximation of the fast wind solutions, and the values of β should be in a restricted interval. To improve the hydrodynamic approximation used in this standard procedure, we have developed two hydrodynamic procedures to derive stellar and wind parameters:

- The self-consistent CAK procedure [44], based on the m-CAK model. Here, we iteratively calculate the line force parameters using the atomic line database from CMFGEN, coupled with the m-CAK hydrodynamic until convergence. We obtain the line force parameters and, therefore, the velocity profile and the mass loss rate. Thus, none of the input parameters are ‘free’, but self-consistently calculated.
- The LambertW procedure [45]. In this procedure, we start using a β -law and a value for \dot{M} in CMFGEN. After convergence, we calculate the line acceleration as a function of r , and, using the LambertW function, we obtain a new velocity profile. This is inserted in CMFGEN and the cycle is repeated until convergence. In this LambertW procedure, the only input parameter is the mass loss rate.

We expect that these two alternatives, which reduce the number of input parameters, will in the future have a significant impact on the standard procedures for obtaining stellar and wind parameters of massive stars.

Author Contributions: M.C. and I.A. participated in all aspects related to this work. All authors have read and agreed to the published version of the manuscript.

Funding: We are grateful for the support from FONDECYT projects 1190485 and 1230131. I.A. also thanks the support from FONDECYT project 11190147. This project has received funding from the European Union’s Framework Programme for Research and Innovation Horizon 2020 (2014–2020) under the Marie Skłodowska-Curie Grant Agreement No. 823734.

Institutional Review Board Statement: Not applicable.

Informed Consent Statement: Not applicable.

Data Availability Statement: Not applicable.

Acknowledgments: We are grateful for the suggestions and comments from reviewers to improve this work. We would like to thank the continuous support from Centro de Astrofísica de Valparaíso and our colleagues and students from the massive stars group at Universidad de Valparaíso, especially Catalina Arcos. We also thank our long-standing colleagues from other institutes who have contributed to our understanding of the field, especially Lydia Cidale, Diego Rial and Roberto Venero. We also wish to acknowledge the support received from our respective Universities, Universidad de Valparaíso and Universidad Mayor, to continue our research.

Conflicts of Interest: The authors declare no conflict of interest.

Abbreviations

The following abbreviations are used in this manuscript:

ZAMS	Zero-Age Main Sequence
EoM	Equation of Motion
CAK	Castor et al. [16]
RHS	Right Hand Side
MMR	Multivariate Multiple Regression
WLR	Wind momentum–Luminosity Relationship
VDD	Viscous Decretion Disc

Appendix A

In their original work, CAK discussed the stellar point approximation of their model and properly estimated the influence of the disc correction factor (CF) on the wind dynamics, i.e., reducing the line force by about 40% at the stellar surface.

The definition of the CF is:

$$CF = \frac{2}{1 - \mu_*^2} \int_{\mu_*}^1 \left(\frac{(1 - \mu^2)v/r + \mu^2 v'}{v'} \right)^\alpha \mu d\mu \quad (A1)$$

where $v' = dv/dr$ and $\mu_*^2 = 1 - (R_*/r)^2$.

Integrating (A1) and changing the variables from $r \rightarrow u = -R_*/r$ and $v \rightarrow w = v/a$, where a is the thermal speed, the finite disc correction factor transforms to:

$$CF(u, w/w') = \frac{1}{1 - \alpha} \frac{1}{u^2} \frac{1}{(1 + \frac{1}{u} \frac{w}{w'})} \left[1 - \left(1 - u^2 - u \frac{w}{w'} \right)^{(1+\alpha)} \right], \quad (A2)$$

where $w' = dw/dr$. Due to the fact that CF depends on u and the ratio $Z = w/w'$, we can define λ as:

$$\lambda = (u + Z) u. \quad (A3)$$

Therefore, $CF(u, Z)$ is re-written as:

$$CF(\lambda) = \frac{1}{(1 - \alpha)} \frac{1}{\lambda} \left[1 - (1 - \lambda)^{(1+\alpha)} \right]. \quad (A4)$$

The partial derivatives of CF with respect to u, w, w' are then related to $\partial CF/\partial \lambda$ via the chain rule, namely:

$$\frac{\partial CF}{\partial u} = \frac{\partial CF}{\partial \lambda} \times \frac{\partial \lambda}{\partial u}. \quad (A5)$$

$$\frac{\partial CF}{\partial w} = \frac{\partial CF}{\partial \lambda} \times \frac{\partial \lambda}{\partial w}. \quad (A6)$$

$$\frac{\partial CF}{\partial w'} = \frac{\partial CF}{\partial \lambda} \times \frac{\partial \lambda}{\partial w'}. \quad (A7)$$

The function $e(\lambda) = \partial CF/\partial \lambda$ is therefore:

$$e(\lambda) = \frac{(1 - \lambda)^\alpha - CF(\lambda)}{\lambda}. \quad (A8)$$

Then, (A5)–(A7) are related to (A8) by:

$$e(\lambda) = \frac{1}{2u + Z} \times \frac{\partial CF}{\partial u} = \frac{w'}{u} \times \frac{\partial CF}{\partial w} = -\frac{w'}{uZ} \times \frac{\partial CF}{\partial w'}. \quad (A9)$$

Approximating Z by a β -field ($Z = (1 + u)/\beta$), we obtain CF and e only as functions of u .

Appendix B

Here, the basic steps toward Equations (52)–(54) are outlined. The reader should keep in mind the original derivation by CAK.

The partial derivatives of $F(u, w, w')$ (Equation (52)), with respect to u, w and w' are:

$$\frac{\partial F}{\partial u} = -\frac{2}{u^2} + a_{rot}^2 - C' \left(\frac{\partial CF}{\partial u} g + CF \frac{\partial g}{\partial u} \right) w^{-\delta} (w w')^\alpha \quad (A10)$$

$$\frac{\partial F}{\partial w} = \left(1 + \frac{1}{w^2} \right) w' - C' \left(\frac{\partial CF}{\partial w} + \alpha \frac{CF}{w} - \delta \frac{CF}{w} \right) g w^{-\delta} (w w')^\alpha \quad (A11)$$

$$\frac{\partial F}{\partial w'} = \left(1 - \frac{1}{w^2} \right) w - C' \left(\frac{\partial CF}{\partial w'} + \alpha \frac{CF}{w'} \right) g w^{-\delta} (w w')^\alpha \quad (A12)$$

After using the new coordinates $Y = w w'$ and $Z = w/w'$, some derivative relation of the correction factor (see Appendix A) and defining:

$$\frac{dg(u)}{du} = g(u) \times h(u) \quad (A13)$$

where

$$h(u) = \delta \left(\frac{2}{u} - \frac{u}{\sqrt{1-u^2}(1-\sqrt{1-u^2})} \right) \quad (A14)$$

the singularity condition ($w' \partial F / \partial w' = 0$) now reads:

$$\left(1 - \frac{1}{YZ} \right) Y - C' f_2(u, Z) g Z^{-\delta/2} Y^{\alpha-\delta/2} = 0 \quad (A15)$$

where $f_1(u, Z) = CF(u, Z)$,

$$f_2(u, Z) = \alpha f_1(u, Z) - u Z \times e(u, Z) \quad (A16)$$

and $e(u, Z) = e(\lambda)$ is defined in Appendix A.

The regularity condition ($Z dF/du = 0$) now transforms to:

$$\left(1 + \frac{1}{YZ} \right) Y - C' f_3(u, Z) g(u) Z^{-\delta/2} Y^{\alpha-\delta/2} = + \frac{2Z}{u^2} - a_{rot}^2 Z \quad (A17)$$

where

$$f_3(u, Z) = (3u + Z) Z \times e(u, Z) + f_1(u, Z) \times (h(u) Z + \alpha - \delta) \quad (A18)$$

Notes

- ¹ The surface gravity g is given in CGS units, i.e., cm/s^2 . The quantity $\log g$ is dimensionless, see Matta et al. [19].
- ² Electrons with a velocity distribution function given by the Maxwellian distribution.
- ³ This equation is for the direct radiation force as no scattering contributions are included within the Sobolev approximation.
- ⁴ The subscript s means at the singular point.

References

1. Johnson, M.C. The emission of hydrogen and helium from a star by radiation pressure, and its effect in the ultra-violet continuous spectrum. *Mon. Not. R. Astron. Soc.* **1925**, *85*, 813–825. [CrossRef]
2. Johnson, M.C. The velocities of ions under radiation pressure in a stellar atmosphere, and their effect in the ultraviolet continuous spectrum (Second paper). *Mon. Not. R. Astron. Soc.* **1926**, *86*, 300. [CrossRef]

3. Milne, E.A. On the possibility of the emission of high-speed atoms from the sun and stars. *Mon. Not. R. Astron. Soc.* **1926**, *86*, 459–473. [\[CrossRef\]](#)
4. Chandrasekhar, I.S. The Time of Relaxation of Stellar Systems. *Astrophys. J.* **1941**, *93*, 285. [\[CrossRef\]](#)
5. Chandrasekhar, S. Stochastic Problems in Physics and Astronomy. *Rev. Mod. Phys.* **1943**, *15*, 1–89. [\[CrossRef\]](#)
6. Spitzer, L. *Physics of Fully Ionized Gases*; Courier Corporation: Chelmsford, MA, USA, 1956.
7. Morton, D.C. The Far-Ultraviolet Spectra of Six Stars in Orion. *Astrophys. J.* **1967**, *147*, 1017. [\[CrossRef\]](#)
8. Lamers, H.J.G.L.M.; Cassinelli, J.P. *Introduction to Stellar Winds*; Cambridge University Press: Cambridge, UK, 1999; p. 219.
9. Snow, T.P.J.; Morton, D.C. Copernicus ultraviolet observations of mass-loss effects in O and B stars. *Astrophys. J. Suppl.* **1976**, *32*, 429–465. [\[CrossRef\]](#)
10. Abbott, D.C. The theory of radiatively driven stellar winds. II—The line acceleration. *Astrophys. J.* **1982**, *259*, 282–301. [\[CrossRef\]](#)
11. Kudritzki, R.P.; Puls, J. Winds from Hot Stars. *Annu. Rev. Astron. Astrophys.* **2000**, *38*, 613–666. [\[CrossRef\]](#)
12. Puls, J.; Vink, J.S.; Najarro, F. Mass loss from hot massive stars. *Astron. Astrophys.* **2008**, *16*, 209–325. [\[CrossRef\]](#)
13. Vink, J.S. Theory and Diagnostics of Hot Star Mass Loss. *Annu. Rev. Astron. Astrophys.* **2022**, *60*, 203–246. [\[CrossRef\]](#)
14. Parker, E.N. Dynamics of the Interplanetary Gas and Magnetic Fields. *Astrophys. J.* **1958**, *128*, 664. [\[CrossRef\]](#)
15. Lucy, L.B.; Solomon, P.M. Mass Loss by Hot Stars. *Astrophys. J.* **1970**, *159*, 879. [\[CrossRef\]](#)
16. Castor, J.I.; Abbott, D.C.; Klein, R.I. Radiation-driven winds in Of stars. *Astrophys. J.* **1975**, *195*, 157–174. [\[CrossRef\]](#)
17. Sobolev, V.V. *Moving Envelopes of Stars*; Harvard University Press: Cambridge, MA, USA, 1960.
18. Castor, J.I. On the force associated with absorption of spectral line radiation. *Mon. Not. R. Astron. Soc.* **1974**, *169*, 279–306. [\[CrossRef\]](#)
19. Matta, C.F.; Massa, L.; Gubskaya, A.V.; Knoll, E. Can One Take the Logarithm or the Sine of a Dimensioned Quantity or a Unit? Dimensional Analysis Involving Transcendental Functions. *J. Chem. Educ.* **2011**, *88*, 67–70. [\[CrossRef\]](#)
20. Hillier, D.J. Hot Stars with Winds: The CMFGEN Code. In *From Interacting Binaries to Exoplanets: Essential Modeling Tools*; Richards, M.T., Hubeny, I., Eds.; IAU Symposium; Cambridge University Press: Cambridge, UK, 2012; Volume 282; pp. 229–234. [\[CrossRef\]](#)
21. Pauldrach, A.W.A.; Hoffmann, T.L.; Lennon, M. Radiation-driven winds of hot luminous stars. XIII. A description of NLTE line blocking and blanketing towards realistic models for expanding atmospheres. *Astron. Astrophys.* **2001**, *375*, 161–195. [\[CrossRef\]](#)
22. Lattimer, A.S.; Cranmer, S.R. An Updated Formalism for Line-driven Radiative Acceleration and Implications for Stellar Mass Loss. *Astrophys. J.* **2021**, *910*, 48. [\[CrossRef\]](#)
23. Friend, D.B.; Abbott, D.C. The theory of radiatively driven stellar winds. III—Wind models with finite disk correction and rotation. *Astrophys. J.* **1986**, *311*, 701–707. [\[CrossRef\]](#)
24. Pauldrach, A.; Puls, J.; Kudritzki, R.P. Radiation-driven winds of hot luminous stars—Improvements of the theory and first results. *Astron. Astrophys.* **1986**, *164*, 86–100.
25. Bjorkman, J.E.; Carciofi, A.C. Modeling the Structure of Hot Star Disks. In *The Nature and Evolution of Disks Around Hot Stars*; Ignace, R., Gayley, K.G., Eds.; Astronomical Society of the Pacific Conference Series; Astronomical Society of the Pacific: San Francisco, CA, USA, 2005; Volume 337; p. 75.
26. Curé, M.; Rial, D.F. A new numerical method for solving radiation driven winds from hot stars. *Astron. Nachrichten* **2007**, *328*, 513. [\[CrossRef\]](#)
27. Curé, M.; Cidale, L.; Granada, A. Slow Radiation-driven Wind Solutions of A-type Supergiants. *Astrophys. J.* **2011**, *737*, 18. [\[CrossRef\]](#)
28. Kudritzki, R.P.; Pauldrach, A.; Puls, J.; Abbott, D.C. Radiation-driven winds of hot stars. VI - Analytical solutions for wind models including the finite cone angle effect. *Astron. Astrophys.* **1989**, *219*, 205–218.
29. Hubeny, I.; Mihalas, D. *Theory of Stellar Atmospheres. An Introduction to Astrophysical Non-equilibrium Quantitative Spectroscopic Analysis*; Princeton University Press: Princeton, NJ, USA, 2015.
30. Santolaya-Rey, A.E.; Puls, J.; Herrero, A. Atmospheric NLTE-models for the spectroscopic analysis of luminous blue stars with winds. *Astron. Astrophys.* **1997**, *323*, 488–512.
31. Puls, J.; Urbaneja, M.A.; Venero, R.; Repolust, T.; Springmann, U.; Jokuthy, A.; Mokiem, M.R. Atmospheric NLTE-models for the spectroscopic analysis of blue stars with winds. II. Line-blanketed models. *Astron. Astrophys.* **2005**, *435*, 669–698. [\[CrossRef\]](#)
32. Hillier, D.J. Modeling the extended atmospheres of WN stars. *Astrophys. Journals* **1987**, *63*, 947–964. [\[CrossRef\]](#)
33. Hillier, D.J.; Miller, D.L. The Treatment of Non-LTE Line Blanketing in Spherically Expanding Outflows. *Astrophys. J.* **1998**, *496*, 407–427. [\[CrossRef\]](#)
34. Hillier, D.J.; Lanz, T. CMFGEN: A non-LTE Line-Blanketed Radiative Transfer Code for Modeling Hot Stars with Stellar Winds. In *Spectroscopic Challenges of Photoionized Plasmas*; Ferland, G., Savin, D.W., Eds.; Astronomical Society of the Pacific Conference Series; Astronomical Society of the Pacific: San Francisco, CA, USA, 2001; Volume 247; p. 343.
35. Hamann, W.R.; Schmutz, W. Computed He II spectra for Wolf-Rayet stars—A grid of models. *Astron. Astrophys.* **1987**, *174*, 173–182.
36. Todt, H.; Sander, A.; Hainich, R.; Hamann, W.R.; Quade, M.; Shenar, T. Potsdam Wolf-Rayet model atmosphere grids for WN stars. *Astron. Astrophys.* **2015**, *579*, A75. [\[CrossRef\]](#)
37. Pozdnyakov, L.A.; Sobol, I.M.; Syunyaev, R.A. Comptonization and the shaping of X-ray source spectra—Monte Carlo calculations. *Astrophys. Space Phys. Res.* **1983**, *2*, 189–331.
38. Roman-Duval, J.; Taylor, J.; Fullerton, A.; Fischer, W.; Plesha, R. *The ULLYSES Large Director's Discretionary Program with Hubble: Overview, Status, and Initial Results*; American Astronomical Society: Washington, DC, USA, 2023; Volume 55, p. 223.02.

39. Hawcroft, C.; Sana, H.; Mahy, L.; Sundqvist, J.O.; de Koter, A.; Crowther, P.A.; Bestenlehner, J.M.; Brands, S.A.; David-Uraz, A.; Decin, L.; et al. X-Shooting ULLYSES: Massive stars at low metallicity. III. Terminal wind speeds of ULLYSES massive stars. *arXiv* **2023**, arXiv:2303.12165. [[CrossRef](#)]
40. Hillier, D.J.; Miller, D.L. Constraints on the Evolution of Massive Stars through Spectral Analysis. I. The WC5 Star HD 165763. *Astrophys. J.* **1999**, *519*, 354–371. [[CrossRef](#)]
41. Noebauer, U.M.; Sim, S.A. Self-consistent modelling of line-driven hot-star winds with Monte Carlo radiation hydrodynamics. *Mon. Not. R. Astron. Soc.* **2015**, *453*, 3120–3134. [[CrossRef](#)]
42. Puls, J.; Springmann, U.; Lennon, M. Radiation driven winds of hot luminous stars. XIV. Line statistics and radiative driving. *Astron. Astrophys.* **2000**, *141*, 23–64. [[CrossRef](#)]
43. Gayley, K.G. An Improved Line-Strength Parameterization in Hot-Star Winds. *Astrophys. J.* **1995**, *454*, 410. [[CrossRef](#)]
44. Gormaz-Matamala, A.C.; Curé, M.; Cidale, L.S.; Venero, R.O.J. Self-consistent Solutions for Line-driven Winds of Hot Massive Stars: The m-CAK Procedure. *Astrophys. J.* **2019**, *873*, 131. [[CrossRef](#)]
45. Gormaz-Matamala, A.C.; Curé, M.; Hillier, D.J.; Najarro, F.; Kubátová, B.; Kubát, J. New Hydrodynamic Solutions for Line-driven Winds of Hot Massive Stars Using the Lambert W-function. *Astrophys. J.* **2021**, *920*, 64. [[CrossRef](#)]
46. Poniatowski, L.G.; Kee, N.D.; Sundqvist, J.O.; Driessen, F.A.; Moens, N.; Owocki, S.P.; Gayley, K.G.; Decin, L.; de Koter, A.; Sana, H. Method and new tabulations for flux-weighted line opacity and radiation line force in supersonic media. *Astron. Astrophys.* **2022**, *667*, A113. [[CrossRef](#)]
47. de Araujo, F.X.; de Freitas Pacheco, J.A. Radiatively driven winds with azimuthal symmetry: Application to Be stars. *MNRAS* **1989**, *241*, 543–557. [[CrossRef](#)]
48. Friend, D.B.; MacGregor, K.B. Winds from rotating, magnetic, hot stars. I. General model results. *Astrophys. J.* **1984**, *282*, 591–602. [[CrossRef](#)]
49. Madura, T.I.; Owocki, S.P.; Feldmeier, A. A Nozzle Analysis of Slow-Acceleration Solutions in One-dimensional Models of Rotating Hot-Star Winds. *Astrophys. J.* **2007**, *660*, 687–698. [[CrossRef](#)]
50. Curé, M. The Influence of Rotation in Radiation-driven Wind from Hot Stars: New Solutions and Disk Formation in Be Stars. *Astrophys. J.* **2004**, *614*, 929–941. [[CrossRef](#)]
51. Araya, I.; Curé, M.; ud-Doula, A.; Santillán, A.; Cidale, L. Co-existence and switching between fast and Ω -slow wind solutions in rapidly rotating massive stars. *MNRAS* **2018**, *477*, 755–765. [[CrossRef](#)]
52. Curé, M. Multi Component Line Driven Stellar Winds. Ph.D. Thesis, Ludwig-Maximilians Universität, Munich, Germany, 1992.
53. Venero, R.O.J.; Curé, M.; Cidale, L.S.; Araya, I. The Wind of Rotating B Supergiants. I. Domains of Slow and Fast Solution Regimes. *Astrophys. J.* **2016**, *822*, 28. [[CrossRef](#)]
54. Rivinius, T.; Carciofi, A.C.; Martayan, C. Classical Be stars. Rapidly rotating B stars with viscous Keplerian accretion disks. *Astron. Astrophys.* **2013**, *21*, 69. [[CrossRef](#)]
55. Araya, I.; Jones, C.E.; Curé, M.; Silaj, J.; Cidale, L.; Granada, A.; Jiménez, A. Ω -slow Solutions and Be Star Disks. *Astrophys. J.* **2017**, *846*, 2. [[CrossRef](#)]
56. Cranmer, S.R.; Owocki, S.P. The effect of oblateness and gravity darkening on the radiation driving in winds from rapidly rotating B stars. *Astrophys. J.* **1995**, *440*, 308–321. [[CrossRef](#)]
57. Kudritzki, R.P. Line-driven Winds, Ionizing Fluxes, and Ultraviolet Spectra of Hot Stars at Extremely Low Metallicity. I. Very Massive O Stars. *Astrophys. J.* **2002**, *577*, 389–408. [[CrossRef](#)]
58. Villata, M. Radiation-driven winds of hot stars—A simplified model. *Astron. Astrophys.* **1992**, *257*, 677–680.
59. Müller, P.E.; Vink, J.S. A consistent solution for the velocity field and mass-loss rate of massive stars. *Astron. Astrophys.* **2008**, *492*, 493–509. [[CrossRef](#)]
60. Araya, I.; Curé, M.; Cidale, L.S. Analytical Solutions for Radiation-driven Winds in Massive Stars. I. The Fast Regime. *Astrophys. J.* **2014**, *795*, 81. [[CrossRef](#)]
61. Araya, I.; Christen, A.; Curé, M.; Cidale, L.S.; Venero, R.O.J.; Arcos, C.; Gormaz-Matamala, A.C.; Haucke, M.; Escárate, P.; Clavería, H. Analytical solutions for radiation-driven winds in massive stars - II. The δ -slow regime. *MNRAS* **2021**, *504*, 2550–2556. [[CrossRef](#)]
62. Corless, R.M.; Gonnet, G.H.; Hare, D.E.G.; Jeffrey, D.J. Lambert's W function in Maple. *Maple Tech. Newsl.* **1993**, *9*, 12–22.
63. Corless, R.M.; Gonnet, G.H.; Hare, D.E.G.; Jeffrey, D.J.; Knuth, D.E. On the LambertW function. *Adv. Comput. Math.* **1996**, *5*, 329–359. [[CrossRef](#)]
64. Cranmer, S.R. New views of the solar wind with the Lambert W function. *Am. J. Phys.* **2004**, *72*, 1397–1403. [[CrossRef](#)]
65. Kudritzki, R.P.; Pauldrach, A.; Puls, J. Radiation driven winds of hot luminous stars. II - Wind models for O-stars in the Magellanic Clouds. *Astron. Astrophys.* **1987**, *173*, 293–298.
66. de Koter, A.; Heap, S.R.; Hubeny, I. On the Evolutionary Phase and Mass Loss of the Wolf-Rayet-like Stars in R136a. *Astrophys. J.* **1997**, *477*, 792. [[CrossRef](#)]
67. Vink, J.S.; de Koter, A.; Lamers, H.J.G.L.M. On the nature of the bi-stability jump in the winds of early-type supergiants. *Astron. Astrophys.* **1999**, *350*, 181–196.
68. Rencher, A.; Christensen, W. *Methods of Multivariate Analysis*; Wiley Series in Probability and Statistics; Wiley: Hoboken, NJ, USA, 2012.

69. Mardia, K.V.; Kent, J.T.; Bibby, J.M. *Multivariate Analysis (Probability and Mathematical Statistics)*; Academic Press: Cambridge, MA, USA, 1980.
70. Kudritzki, R.P.; Bresolin, F.; Przybilla, N. A New Extragalactic Distance Determination Method Using the Flux-weighted Gravity of Late B and Early A Supergiants. *Astrophys. J.* **2003**, *582*, L83–L86. [\[CrossRef\]](#)
71. Kudritzki, R.P.; Urbaneja, M.A.; Bresolin, F.; Przybilla, N.; Gieren, W.; Pietrzyński, G. Quantitative Spectroscopy of 24 A Supergiants in the Sculptor Galaxy NGC 300: Flux-weighted Gravity-Luminosity Relationship, Metallicity, and Metallicity Gradient. *Astrophys. J.* **2008**, *681*, 269–289. [\[CrossRef\]](#)
72. Ekström, S.; Georgy, C.; Eggenberger, P.; Meynet, G.; Mowlavi, N.; Wyttenbach, A.; Granada, A.; Decressin, T.; Hirschi, R.; Frischknecht, U.; et al. Grids of stellar models with rotation. I. Models from 0.8 to 120 M_{\odot} at solar metallicity ($Z = 0.014$). *Astron. Astrophys.* **2012**, *537*, A146. [\[CrossRef\]](#)
73. Kudritzki, R.; Lennon, D.J.; Puls, J. Quantitative Spectroscopy of Luminous Blue Stars in Distant Galaxies. In *Proceedings of the Science with the VLT*; Walsh, J.R., Danziger, I.J., Eds.; Springer: Berlin/Heidelberg, Germany, 1995; p. 246.
74. Gormaz-Matamala, A.C.; Curé, M.; Lobel, A.; Panei, J.A.; Cuadra, J.; Araya, I.; Arcos, C.; Figueroa-Tapia, F. New self-consistent wind parameters to fit optical spectra of O-type stars observed with the HERMES spectrograph. *Astron. Astrophys.* **2022**, *661*, A51. [\[CrossRef\]](#)
75. Porter, J.M.; Rivinius, T. Classical Be Stars. *Publ. Astron. Soc. Pac.* **2003**, *115*, 1153–1170. [\[CrossRef\]](#)
76. Bjorkman, J.E.; Cassinelli, J.P. Equatorial disk formation around rotating stars due to Ram pressure confinement by the stellar wind. *Astrophys. J.* **1993**, *409*, 429–449. [\[CrossRef\]](#)
77. Owocki, S.P.; Cranmer, S.R.; Gayley, K.G. Inhibition FO Wind Compressed Disk Formation by Nonradial Line-Forces in Rotating Hot-Star Winds. *Astrophys. J.* **1996**, *472*, L115. [\[CrossRef\]](#)
78. Lee, U.; Osaki, Y.; Saio, H. Viscous excretion discs around Be stars. *Mon. Not. R. Astron. Soc.* **1991**, *250*, 432–437. [\[CrossRef\]](#)
79. Okazaki, A.T. Viscous Transonic Decretion in Disks of Be Stars. *Publ. Astron. Soc. Jpn.* **2001**, *53*, 119–125. [\[CrossRef\]](#)
80. Krtićka, J.; Owocki, S.P.; Meynet, G. Mass and angular momentum loss via decretion disks. *Astron. Astrophys.* **2011**, *527*, A84. [\[CrossRef\]](#)
81. Curé, M.; Meneses, R.; Araya, I.; Arcos, C.; Peña, G.; Machuca, N.; Rodriguez, A. Revisiting viscous transonic decretion disks of Be stars. *Astron. Astrophys.* **2022**, *664*, A185. [\[CrossRef\]](#)
82. Silaj, J.; Curé, M.; Jones, C.E. Line-Driven Winds Revisited in the Context of Be Stars: Ω -slow Solutions with High k Values. *Astrophys. J.* **2014**, *795*, 78. [\[CrossRef\]](#)
83. Lamers, H.J.G.L.M.; Snow, T.P.; Lindholm, D.M. Terminal Velocities and the Bistability of Stellar Winds. *Astrophys. J.* **1995**, *455*, 269. [\[CrossRef\]](#)
84. Vink, J.S. Fast and slow winds from supergiants and luminous blue variables. *Astron. Astrophys.* **2018**, *619*, A54. [\[CrossRef\]](#)
85. Vink, J.S.; Sander, A.A.C. Metallicity-dependent wind parameter predictions for OB stars. *Mon. Not. R. Astron. Soc.* **2021**, *504*, 2051–2061. [\[CrossRef\]](#)
86. Stahl, O.; Wolf, B.; Aab, O.; Smolinski, J. Stellar wind properties of A-type hypergiants. *Astron. Astrophys.* **1991**, *252*, 693–700.
87. Lefever, K.; Puls, J.; Aerts, C. Statistical properties of a sample of periodically variable B-type supergiants. Evidence for opacity-driven gravity-mode oscillations. *Astron. Astrophys.* **2007**, *463*, 1093–1109. [\[CrossRef\]](#)
88. Markova, N.; Puls, J. Bright OB stars in the Galaxy. IV. Stellar and wind parameters of early to late B supergiants. *Astron. Astrophys.* **2008**, *478*, 823–842. [\[CrossRef\]](#)
89. Haucke, M.; Cidale, L.S.; Venero, R.O.J.; Curé, M.; Kraus, M.; Kanaan, S.; Arcos, C. Wind properties of variable B supergiants. Evidence of pulsations connected with mass-loss episodes. *Astron. Astrophys.* **2018**, *614*, A91. [\[CrossRef\]](#)
90. Rivet, J.P.; Siciak, A.; de Almeida, E.S.G.; Vakili, F.; Domiciano de Souza, A.; Fouché, M.; Lai, O.; Vernet, D.; Kaiser, R.; Guerin, W. Intensity interferometry of P Cygni in the $H\alpha$ emission line: Towards distance calibration of LBV supergiant stars. *MNRAS* **2020**, *494*, 218–227. [\[CrossRef\]](#)

Disclaimer/Publisher’s Note: The statements, opinions and data contained in all publications are solely those of the individual author(s) and contributor(s) and not of MDPI and/or the editor(s). MDPI and/or the editor(s) disclaim responsibility for any injury to people or property resulting from any ideas, methods, instructions or products referred to in the content.